Spring 1997

Wind Climatology at 87 km above the Rocky Mountains at Bear Lake Observatory--Fabry-Perot Observations of OH

V. B. Wickwar
Utah State University

I K. Monson
Utah State University, Novell Corporation

C M. Vadnais
Utah State University, U.S. Airforce

D Rees
Utah State University

Wind Climatology at 87 km above the Rocky Mountains at Bear Lake Observatory—Fabry-Perot Observations of OH

V.B. Wickwar[1], I.K. Monson[1,2], C.M. Vadnais[1,3], D. Rees[1]

[1] Utah State University
[2] Novell Corporation
[3] U.S. Air Force

Utah State University
Center for Atmospheric and Space Sciences
Logan, UT 84322-4405

Wind Climatology at 87 km above the Rocky Mountains at Bear Lake Observatory—Fabry-Perot Observations of OH

Vincent B. Wickwar[1], Ian K. Monson[1,2], Carolyn M. Vadnais[1,3], David Rees[1]

[1]Center for Atmospheric and Space Sciences, Utah State University, Logan, UT 84322-4405
[2]Current address: Novell, Inc., PRV B16, 122 East 1700 South, Provo, UT 84606-6194
[3]Current address: Armstrong Laboratories, Tyndall AFB, FL 32403

Abstract. This paper presents the neutral-wind climatology at approximately 87-km altitude from Utah State University's Bear Lake Observatory (BLO), a mid-latitude site situated in the middle of the Rocky Mountains. The winds were determined using a very sensitive Fabry-Perot interferometer (FPI) observing the OH Meinel (6-2) $P_1(3)$ line at 843 nm. The climatology, determined from monthly averages of the nightly evolution of the geographic meridional and zonal wind components over forty-five months, has three distinct seasonal patterns: *winter* (November–February), *summer* (May–July), and *late summer* (August and September). The background zonal wind is eastward the whole year except March and April. The background meridional wind is northward in *winter* and southward during the rest of the year. In *late summer*, the winds exhibit a very strong semidiurnal tidal variation almost every night. In *summer*, they exhibit a similar tidal variation on enough nights that a semidiurnal pattern appears in the climatology. In *winter*, the night-to-night variability is so great that little structure is evident in the climatology. These winds are compared to those from other techniques or sites: HRDI observations from UARS, FPI observations from Michigan, and MF radar observations. While generally agreeing in relative amplitudes and in phase, differences do exist, especially the weak semidiurnal tide at BLO in *winter* and a greatly reduced tide at spring equinox compared to *late summer*. It is likely that these differences arise from the

topographical generation of gravity waves by winds flowing over the Rocky Mountains. The tidal variations are also compared to results from the global-scale wave model (GSWM): our semidiurnal amplitudes are considerably bigger except in winter, and our phases vary from showing very good agreement in July, fair agreement in April and January, and disagreement in October. These large differences may be evidence that non-linear effects are more important than realized. The behavior of the background winds is consistent with different populations of gravity waves reaching 87 km in *summer* and *winter*. The behavior of the semidiurnal tidal variation is consistent with a strong interaction between the tidal and gravity-wave wind fields, and is consistent with the different *summer* and *winter* gravity wave populations, and with a fall-spring asymmetry characterized by much weaker gravity wave sources in *late summer* than near spring equinox.

1. Introduction

The nighttime airglow emission from OH reflects the state of the upper mesosphere near the mesopause, which in turn reflects many radiative, chemical, and dynamical processes that occur between the troposphere and lower thermosphere. We usually think of the peak of the OH emission layer as being at 87-km altitude and having a full thickness at half-maximum intensity of 6 km [*Baker and Stair*, 1988; *von Zahn et al.*, 1987]. In close agreement, recent OH observations from UARS near the northern hemisphere spring equinox show a peak altitude of 88 km for most of the night [*Lowe et al.*, 1996]. At 87 km, the emission peak is located at essentially the mid-latitude mesopause in summer and approximately 15 km below the mesopause in winter [*Chanin et al.*, 1987; *Hauchecorne et al.*, 1991; *Senft et al.*, 1994; *Wickwar et al.*, 1997a]. Accordingly, the temperature goes through a large annual cycle with a hot winter and cold summer.

The atmospheric region within which the OH emission occurs is affected either directly or indirectly by dynamical features on just about every time and spatial scale. The temperature variation is related to a large-scale, meridional circulation from summer to winter, i.e., in the northern hemisphere it is from north to south in summer and from south to north in winter [e.g., *Murgatroyd*, 1957; *Geller*, 1983; *Hedin et al.*, 1996]. It is undoubtedly affected by the large-scale, mesospheric, temperature inversion-layer phenomenon that is particularly prevalent in winter at lower altitudes in the mesosphere [e.g., *Hauchecorne et al.*, 1987; *Whiteway et al.*, 1995]. The inversion layers have a characteristic duration of one to two weeks and with infrequent sampling can give rise to what appears to be a large interannual winter variation [e.g., *Wickwar et al.*, 1997a]. The particularly strong winter inversion layers also appear to be closely related to stratospheric warmings and planetary waves [e.g., *Hauchecorne and Chanin*, 1982; 1983]. For shorter periods—24, 12, 8, 6, hours, etc.—the emission region is affected by tides [e.g., *Rees et al.*, 1990] from the insolation absorbed in stratospheric O_3 and tropospheric water vapor [e.g., *Hagan et al.*, 1995]. For still shorter periods—minutes to a few hours—the region is affected by gravity waves [e.g., *Swenson and Mende*, 1994; *Wu and Killeen*, 1996]. They can be generated in the troposphere by a number of sources: winds flowing over the Rocky Mountain topography [e.g., *Nastrom and Fritts*, 1992; *Bacmeister*, 1993], convective storms [e.g., *Alexander* *et al.*, 1995; *Alexander*, 1996], and the jet stream [e.g., *Fritts and Nastrom*, 1992; *Murayama et al.*, 1994a; *Tsuda et al.*, 1994].

Thus the dynamics of the OH-emission region will reflect the integrated effect of all these processes and phenomena, as well as others. In this paper we examine the effects, i.e., the time dependence of the nighttime winds above one mid-latitude location. This is the type of study that is ideally suited for ground-based observations. To do this we use observations from an extremely sensitive Fabry-Perot interferometer (FPI). Initial results have been presented by *Rees et al.* [1990] and *East et al.* [1995], demonstrating the feasibility of obtaining the time evolution of the winds with good precision with this instrument. This paper uses data from four years (45 months) to determine the wind climatology. To help understand it, we also investigate the year-to-year and night-to-night variability. The latter is a particular strength of this instrument—the ability to determine accurate and precise winds during the night. The climatology apparent in these monthly averages shows several distinct periods, each with a different wind pattern. In traditional fashion we call these periods seasons, but these "observed" seasons differ from any of the definitions in common use. To account for this climatology will require an understanding of the middle atmosphere, including the generation of several types of waves, their filtering, their interactions, and their saturation. More immediately, this work contributes to the international MLTCS (Mesosphere, Lower-Thermosphere, Coupling Study) program and the CEDAR LTCS program, to the UARS (Upper-Atmosphere Research Satellite) correlative measurements program, and to the MSX (Mid-Course Space Experiment) mission. In the future, this instrument and this work will be available to contribute to the PSMOS (Planetary Scale

Mesopause Observing System) program and the TIMED (Thermosphere-Ionosphere-Mesosphere Energetics and Dynamics) mission.

In the next section, we describe the FPI and the reduction of the data to winds. In Section 3, we describe the winds as well as the inferred background winds and semidiurnal variations. In Section 4, we summarize these wind results and compare them to other wind observations and GSWM calculations. In Section 5, we relate the seasonal variations of both the background winds and the semidiurnal tides to what we know about gravity waves, including a climatology of the low-altitude wind over the mountains in northern Utah. In Section 6, we give our conclusions, a major part of which is a model of the mid-latitude, middle atmosphere needed to account for the observed winds and tides.

2. Instrumentation and Data Reduction

The observations were made from the Bear Lake Observatory (BLO) (41.93° N, 111.42° W, 2 km altitude), located near Garden City, UT, which is on the edge of Bear Lake. This location is relatively close to Utah State University (USU) for convenient access—61 km by road or 39 km line-of-sight—yet rural enough to have a very low background light level. The building is a converted 12-by-70-foot trailer that has been remodeled and added onto to create and support eight instrument bays. This addition includes a loading dock, an indoor staircase to the roof, a bathroom, a small kitchen, and a storage area. BLO currently houses the Fabry-Perot interferometer (FPI) used for these observations, a dynasonde, an all-sky imager, an

OH temperature mapper, a Michelson interferometer, a magnetometer, and a weather station. At USU, correlative observations can also be obtained with a Rayleigh-scatter lidar [*Wickwar et al.*, 1997a, 1997b; *Gao et al.*, 1997; *Sears et al.*, 1997] and, in the future, with a resonance-scatter lidar [*Wickwar et al.*, 1996; *Collins et al.*, 1997]. Other instruments have been located there for special campaigns [e.g., *Swenson and Mende*, 1994; *Weins et al.*, 1995], and other instruments are welcome for campaigns and long-term correlative observations. The instruments are easily accessed by telephone.

Observations of the OH Meinel (6-2) $P_1(3)$ line at 843 nm were made with an imaging Fabry-Perot interferometer, Figure 1, developed by one of the authors (D.R.) at Hovemere, Ltd. [*Rees et al.*, 1989]. It uses 15-cm, $\lambda/200$, thermally-controlled plates with 20.49-mm zerodur spacers; a 5-position filter wheel for 2-inch filters; an ITT imaging photon detector (IPD) with a 25-mm, GaAs photocathode, and a resistive anode; a Peltier cooler; and a constant-temperature, water-glycol heat exchanger. The etalon chamber is slightly evacuated, the effective f-number of the system is 10, and the detector is thermoelectrically cooled to –30° C. Approximately one free spectral range of the FPI is imaged onto the IPD. The OH filter is centered at 843.2 nm and is 1.0-nm wide. There is also a red-line filter, centered at 630.2 nm and 0.5-nm wide, for thermospheric observations of $O(^1D)$ [e.g., *Wickwar et al.*, 1997c]. The usual integration time in each position is four minutes, which is enough to obtain wind and temperature uncertainties [this paper; *Choi et al.*, 1997a, b] that are as small as those obtained with a bare CCD [e.g., *Niciejewski and Killeen*, 1995].

Returning to the optical properties of the FPI, the etalon has a free spectral range of 7.32 GHz and a resolution of 244 MHz for a nominal finesse of 30. Under the best of conditions, the center position is found to one percent of that, corresponding to a *precision* of ±2 m/s at 843 nm. There are controllers for the etalon temperature, the IPD, the filter wheel, and an RF-excited calibration lamp. Through these and computer control, the FPI is fully automated to run unattended every night for months. The observing bay in the observatory is temperature controlled to 21±2° C, and a high volume of this warm air is continually circulated into the area under the observing dome. Light from an RF-excited source is observed during every sequence of azimuth positions to monitor instrument stability. Strongly diffused light from a light bulb is observed every few months to make flat-field calibrations, and strongly diffused light from a single-mode He-Ne laser is observed every few months at many etalon-chamber pressure settings to determine the instrument function. This detailed calibration information has been used to determine the OH temperatures during a two-year period [*Choi et al.,* 1997a, 1997b].

The data reduction starts during the data acquisition when the two-dimensional fringe pattern is integrated to make a one-dimensional spectrum that is linear in wavelength. It is more efficient to store this spectrum instead of the two-dimensional fringe pattern, and was the only affordable option in 1989 when this instrument was developed. However, this approach requires a good knowledge of the location of the center of the fringe. (In the long run it would be preferable to store the fringe pattern. Technologically, this is now feasible with large, high-speed disks, digital tapes, and CD-ROM writers) Off line, the basic reduction procedure involves subtracting the thermionic emission, correcting the signal for variations in sensitivity of the detector over its surface area (flat-field correction), fitting the observed one-dimensional spectrum with a Fourier series, recreating that spectrum using just the low-frequency terms, and determining the location of the emission peak. The data reduction also involves finding the zero-

Doppler position by comparing the peak positions from observing in four pairs of opposite directions and the zenith over the course of many nights, and relating that mean position to the position of the emission from a calibration lamp. This then enables the Doppler shifts to be determined, and from these shifts the line-of-sight (LOS) speeds and the vector velocities. This data reduction procedure is discussed more extensively by *Vadnais* [1993] and *Monson* [1997] However, because pairs of observations in opposite directions are used, as described shortly, to find an averaged vector velocity, the determination of the zero-Doppler position is not critical. This is easiest to understand by considering observations to the east and west. As long as the flow is *spatially uniform* over the FPI field of regard, *steady* during the time between the two observations, and the instrument *does not drift* between the two observations, then the wavelength difference between the two spectra is twice the Doppler shift. This possibility of using relative Doppler shift to find the vector velocity assures the *accuracy* of the results. Furthermore, a comparison of the north and east velocity components from the vector velocity to the LOS speeds in the corresponding four cardinal directions provides a reliable indication of whether or not the zero-Doppler position has been found accurately.

Another essential part of the data reduction is to determine the presence or absence of clouds by examining several aspects of the data and other information. The procedure is largely based on the difference in signals observed along LOSs in the zenith direction and at a 30° elevation angle. Under clear conditions, the van Rhijn effect gives rise to a much stronger signal from both the OH airglow and the background continuum at the 30° elevation angle than in the zenith. Under cloudy conditions, the multiple scattering of the OH airglow and background continuum in the cloud layer tends to equalize the signals at the two elevation angles. As the clouds become thicker, the Doppler shifts from all directions approach zero, and eventually the signals approach zero. When the moon is three-quarters full and there are thin clouds, the behavior is very different. The background can increase so much from scattered moonlight that the data become unusable. Yet there are occasions when it is so clear that good observations can be made the day before or after a full moon. The cloud detection procedure is discussed in more detail in *Vadnais* [1993] and *East et al.* [1995].

Figure 2 illustrates the results of this data reduction procedure, showing the various parameters deduced for 14 September 1993 as a function of UT (0000–1400 UT corresponds to 1700–0700 LT, where the LT is U.S. Mountain Standard Time, and 1635–0635 LST, local solar time). The top two panels show relative intensities. There are eight curves for the observations at a 30° elevation angle and equally spaced azimuths, and one for the zenith observations. (Because very good LOS speeds can be obtained in only four minutes it was decided to observe in eight positions instead of the more usual four to obtain more complete spatial information.) The next four panels show the resulting four pairs of oppositely directed LOS speeds. If the neutral velocity over the 300-km diameter circle (at 87-km altitude) sampled by the FPI were uniform, then the solid and dashed curves would be mirror images of each other in each panel. Although not perfectly uniform, this velocity field does show a strong tendency toward mirror images. Uncertainties are shown for each observation. When the moon is up and one of the directions would cause the FPI to look at or close to the moon, that position is skipped. This would show up as a gap in some of the intensities and LOS speeds. The last two panels show the deduced vector velocities in meters per second. They are derived from the LOS speeds by linearly interpolating them to a common time and fitting them in a least-squares sense. For better displays and for convenience in creating the climatology, we interpolate the observations to times 15-

minutes apart, starting on the hour. However, we need to keep in mind that the acquisition time for a full set of independent samples is 40 minutes, not 15 minutes.

Because eight positions are used, it is possible to examine the uniformity of the wind field. Instead of fitting all eight LOS speeds in a least-squares sense to derive an average vector, we use sets of three adjacent LOS speeds to derive the vector wind in different parts of the sky. For instance, observations to the northwest, north, and northeast can be combined to estimate the vector wind in the north; observations to the north, northeast, and east can be combined to estimate the vector wind in the northeast. For this procedure, the zero-Doppler position has to be well determined. An example of this procedure applied to the OH observations on 5 September 1994 is shown in Figure 3. This figure shows maps of the vector velocities at approximately 40-minute intervals. On this day the flow pattern over BLO is extremely uniform and rotates in a clockwise direction during the night with a 12-hour period.

3. Observations

The OH observations at BLO started at the end of August 1989 and have continued to the present. They have been continuous except for an 18-month period (April 1990 to November 1991) when a detector failed and a few short periods when other equipment problems occurred. During most of this period, observations alternated in various patterns between OH and $O(^1D)$. The data discussed in this paper were acquired in September 1989, and between November 1991 and June 1995. During this 45-month period, good OH observations were obtained in every month, with contributions to the climatology coming from 358 nights. A monthly summary is given in Table 1. The quality of the data throughout the period was very uniform, with the exception of a period between January and October 1992 when an electronic drift caused the center of the fringe pattern to drift during the night. Consequently, these 1992 data have been examined especially carefully and extensively to determine their validity. What we found is that the 1992 vector velocities we are using in this paper are good, but the individual LOS speeds that depend critically on the zero-Doppler position are compromised. As stated earlier, speeds derived from measurements made in opposite directions do not depend on the zero-Doppler position, provided the flow pattern is uniform in space and constant in time between the two observations, and the zero-Doppler position does not drift significantly in that same time interval. This great simplification extends to our determination of vector velocities from viewing in four pairs of opposite directions However, our determination of the error bars for the LOS speeds takes the drift of the zero-Doppler position into account in a very conservative fashion. This gave rise to very large error bars on the LOS speeds during this 10-month period in 1992, which were propagated through the vector-velocity calculations, giving rise to unrealistically large error bars for the meridional and zonal winds. Proper values would be closer to those shown for the other time periods. Normally, variations in the error bars mostly reflect variations in the OH emission and background intensities.

The wind climatology, consisting of monthly-averaged winds at 15-minite intervals, is shown in Figure 4. Based on the diurnal variation of the average wind, the direction of the wind, and the day-to-day variability, the climatology can be divided into three distinct periods or seasons and two short transition periods. The seasons are *summer, late summer*, and *winter* as indicated in Table 2 and Figure 4. (We are using italics to distinguish the observation-based seasons from the usual seasons.) The distinct transition periods are October, and March–April. These seasons do not conform to any of our usual astronomical definitions, either those centered on the solstices and equinoxes or those beginning on the solstices and equinoxes. We avoided the word "autumn" in favor of "*late* *summer*" because there is no period with a similar behavior that could be called "spring." Thus these seasons based on the behavior of the winds at 87 km exhibit a major fall-spring asymmetry having no equivalent of two equinoxes.

3.1. *Late Summer*

The most dramatic period for the OH winds is *late summer*, which as previously noted [*Rees et al.*, 1990] is dominated by what appears to be a very strong semidiurnal variation. This interpretation is strongly supported by the time variation of the two components being nearly sinusoidal with a 12-hour period, the two components exhibiting quadrature with the meridional component leading the zonal by approximately three hours, and the two components having almost the same amplitude. The behavior of the two components leads to a clockwise rotation of a nearly constant magnitude wind vector that is clearly visible in the hodogram in Figure 2 and in the vectors in Figure 3. Being derived from a long average, as opposed to a two or three-day average, this semidiurnal variation represents a semidiurnal tide [e.g., *Vial*, 1993]. The amplitudes (in m/s) and phases (in LST in hours) for the two *late summer* months are given in Table 3. Using September as an example, the phases and amplitudes were deduced in the following manner. The time of the smallest wind observation is found in two ways and averaged. The time of the actual meridional minimum is 0515 UT. The midtime between identical winds measured at least an hour before and after the minimum is 0445 UT. That gives an average of 0500 UT. Because the "phase" refers to a maximum, not a minimum, we add six hours to the minimum and then subtract 7.43 hours to convert it to LST. In this case we could verify the semidiurnal variation from the wind maximum just before dawn. Its time minus six hours is 0512, in close agreement to the two times for the minimum. The amplitude was found by assuming the wind to be a sinusoid and averaging together suitable scaled values (when available) from ±2 hours (±60°)

about the symmetric point (i.e., about 0445 UT in this example), ±3 hours (±90°), ±4 hours (±120°), and ±5 hours (±150°). When available, these results were usually very consistent with one another.

Combining the results from the two months to obtain a seasonal average, the meridional amplitude and phase are 27 m/s and 0336 LST, and the zonal amplitude and phase are 24 m/s and 0612 LST.

In addition to the semidiurnal variation, we see in Figure 4 that the two components are asymmetric about the zero line, more so for August than September. Assuming a small-to-negligible diurnal tide, this asymmetry implies a net southward meridional wind (a flow from north to south) and an eastward zonal wind (a flow from west to east). This same conclusion of a semidiurnal variation superimposed on a southward meridional wind and eastward zonal wind is also well demonstrated for an individual day in the hodogram in Figure 2. (This effect is not subtle.) The background wind is found by adding the semidiurnal tidal amplitude to the minimum wind speed used in the amplitude calculation. The results are given in Table 3.

Combining the two results for *late summer*, the background winds are 4 m/s towards the south and 10 m/s towards the east. However, as clearly seen in Figure 4, both components are significantly stronger in August than in September.

The left-hand part of Figure 5 shows the monthly-averaged diurnal wind variations for September for three separate years. With fewer days included in the averages than in Figure 4, the curves are noisier. However, they clearly show a very similar wind pattern from year to year, as well as an interannual variation. The amplitudes are definitely stronger in 1989 and 1993 than in 1992. In particular, the meridional amplitudes in 1992 and 1993 are 22 m/s and 36 m/s, respectively.

Figure 6 shows examples of diurnal variations for six September nights. The days were chosen to show major *departures* from the averages. What is remarkable is how similar they are, with the exception of 8 September 1993, to one another and to the averages. (We do not find anything like this degree of nightly similarity in the other seasons.) One difference among the days is a variation in the semidiurnal amplitudes on individual nights. Both 4 September 1989 and 14 September 1993 exhibit extremely large meridional amplitudes of approximately 50 m/s. This drops to approximately 30 m/s on 6 September 1989 and 12 September 1993. However, when the amplitude of the variation drops even more, as on 8 September 1993, the variation is no longer as clearly semidiurnal: the two components have different amplitudes and the phase quadrature is missing. Another difference from day to day is a large variation in the background winds. Still assuming a small-to-negligible diurnal tide, we find a meridional velocity of 20 m/s toward the south on 11 September 1989 and 0 m/s on 14 September 1993. While the zonal velocity is harder to evaluate, it appears to be small or westward on 12 September 1993, whereas it appears to be eastward on all the other days.

3.2. *Summer*

The next period with a distinct pattern is *summer*. Again, the wind variation appears to be sinusoidal, but because of the shortened observing period—only six hours—it is harder to tell what is happening than in the *late summer*. However, a basic similarity in appearance to the wind pattern in *late summer*, suggests that there is a strong semidiurnal tidal variation.

Examining the pattern in more detail, the meridional winds show distinct minima between 0530 and 0700 UT, and the zonal winds show minima near the end of the observations between 0900 and 1000 UT. The three-hour time difference for the minima in the meridional and zonal components is suggestive of phase quadrature for a wind dominated by a strong semidiurnal tide. Furthermore, the timing of these minima implies a slow phase progression towards earlier times from the *summer* period through, as we will see, the October transition period, i.e., there is a gradual trend rather than a discontinuous change. Finally, the changes in the two deduced wind components are within a factor of two of having the same amplitude. Thus the quadrature, continuous phase shifts, and inferred similar amplitudes of the two components strongly suggest that the average *summer* behavior has at least a very strong contribution from a semidiurnal tide.

The minima were found as in *late summer*. The amplitudes were found using multiple values between 1½ hours (45°) and 4½ hours (135°) from the time of the minimum determined by symmetry. The results for the three *summer* months are given in Table 3. For the *summer*, the mean meridional amplitude of 17 m/s and zonal amplitude of 11 m/s are approximately half those of *late summer*. The mean meridional phase at 0444 LST and mean zonal phase at 0746 LST are more than an hour later than for *late summer*.

Continuing to assume that this semidiurnal variation dominates the temporal variation of the observed winds, we can estimate the magnitudes of the background winds. To do so, we use the observed minima and the deduced amplitudes of the semidiurnal tide. The results are given in Table 3. For the *summer*, the mean meridional wind is 10 m/s towards the south and the mean zonal wind is 12 m/s towards the east. These deduced winds are in the same direction as in *late* *summer*, but the magnitude of the meridional component is more than twice as large, while the zonal component is only slightly larger.

The middle part of Figure 5 shows the monthly-averaged wind variations for June for three years in a row, 1992–1994. They show very similar wind patterns from year to year as well as an interannual variation. June 1993 stands out from the others because of a much larger semidiurnal variation than in the other two years. It is also associated with a larger background eastward wind. While June 1992 and 1994 have similar appearances, the background eastward wind is stronger in 1994.

Figure 7 shows examples of diurnal variations for six *summer* nights between the end of May and early July. As for Figure 6 for *late summer*, these nights were chosen to show major departures from the averages. However, unlike the situation in *late summer*, the winds on the individual nights do not look like the averages. In fact, very few of the individual nights in the *summer* period do. Nonetheless, month-long averages produce very similar patterns from month to month and year to year, as we have already seen.

For the nights in Figure 7, several features stand out. The meridional wind is usually strongly towards the south and the zonal wind strongly towards the east, as in the averages. However, 24 June 1992 is a notable exception, appearing like the April average with a strong zonal wind towards the west. Three of the nights (19 June 1993, 8 July 1992, and 10 July 1993) appear to have higher-frequency components than semidiurnal and have different phase relationships between the two components. Unlike *late summer*, considerable day-to-day variation exists in the *summer* winds such that we can find six nights that do not look like the averages. Nonetheless, multiday averages of the *summer* data give rise to a clear and strong semidiurnal pattern.

3.3. *Winter*

The third period with a distinct pattern is *winter*. In the previous two periods, the observed variation appeared to be semidiurnal. Despite the much longer observing period in *winter*, it is much harder to discern a semidiurnal pattern. The amplitudes of variations in the averaged winds are much smaller, between 5 and 10 m/s. If there were a semidiurnal or other oscillation, it would be very small. In November there is a hint of a semidiurnal oscillation, but the minima and maxima are not well-formed. In December and January, there appears to be a small semidiurnal oscillation that is consistent from one month to the next. In February, there is a hint of oscillations, but they appear to have shorter periods. Possible phase values imply multi-hour phase jumps between successive months in the time interval between October and February. We will return to this later. In addition, the right-hand part of Figure 5 shows the monthly-averaged diurnal wind variations for January for three separate years. The meridional wind, in particular, shows a minimum at a different time each year. Nonetheless, a consistent pattern does appear to emerge with the four-year averages for December and January. There are reasonably clear minima in both components. Amplitudes can be estimated for the zonal wind from its value six hours earlier, and for the meridional wind from its variation with phase angle about the minimum. The results are given in Table 3. The mean meridional phase is 6.1 LST and the amplitude 5 m/s. The mean zonal phase is 9.8 LST and the amplitude 8 m/s. Confidence in the interpretation comes from the similarity in behavior of the two months, the approximate phase quadrature, and the similar amplitudes of the two components.

At this time it is not possible to deduce parameters for a semidiurnal variation in November and February. Accordingly no phases or amplitudes are given in Table 3.

Within the 11–12 hour observing window, definite statements can be made about the background winds. In all four *winter* months the meridional component is almost always towards the north and the zonal component almost always towards the east. As already noted, the variations are relatively small. We estimated the background winds for December and January by adding the semidiurnal amplitudes to the meridional and zonal minima. These values are given in Table 3. We also estimated the background winds for all four months by averaging the appropriate component throughout the night. The results for November and February are given in Table 3. If there were a semidiurnal component, we would average it out in the long observing window. Very encouragingly, the results for December and January differ by less than 1 m/s for the two techniques. These are good estimates provided any diurnal tide is small. The mean *winter* meridional wind is 7 m/s towards the north and the mean zonal wind is 6 m/s towards the east. The meridional component is in the opposite direction to what is observed in all other months of the year. The magnitude is less than is observed in *summer*, but more than is observed in *late summer*. The zonal component is in the same direction as in the other two seasons, but has a smaller magnitude. Thus the *winter* period is characterized, at least at night, by a small meridional wind to the north and a small zonal wind to the east. The absence of a semidiurnal tide or the presence of a very small one and the presence of a northward meridional wind set *winter* apart from the other seasons.

Returning to Figure 5, the individual Januarys are similar to the multiyear averaged January in that the background wind is small and to both the north and to the east. However, the diurnal variation is different from year to year. This interannual variation in the averages might arise from our sampling or from underlying differences from year to year. In view of the great interannual differences seen in mesospheric temperature profiles [*Wickwar et al.*, 1997a and b], we infer that these interannual wind differences are probably real.

The diurnal variation is shown in Figure 8 for six *winter* nights between late December and the end of January. As for Figures 6 and 7, the nights were chosen to show major departures from the averages. It is apparent that great night-to-night variability is the hallmark of this period. The wind can appear to be entirely to the east during one night (27 December 1991) or entirely to the west during another (12 January 1992), a 12-hour period during one night (28 December 1991) or an 8-hour period during another (9 January 1992), and speeds exceeding 50 m/s during one night (31 January 1994) or below 25 m/s during another (19 January 1994). A further indication of the variability is the contrast between adjacent nights (27 and 28 December 1991).

The 28 December 1991 night is also interesting because of the semidiurnal variation mentioned above and the similarity of the magnitudes of the meridional and zonal components to those seen in Figure 6 for *late summer*. The phases on this night are approximately three hours later than in *late summer*, and one to two hours later than in *summer*. They are very similar to the phases found in the four-year average. This suggests that the semidiurnal variation is excited almost equally well in *winter* as in *late summer* and can, under the "right" conditions, propagate to 87-km altitude though with a different phase because of differences in the generation and propagation. However, the great variety of observed patterns in *winter* suggests that the original tidal pattern is strongly modified, on most days, between where it is generated and 87 km. It appears to be so heavily modified that considerable averaging is required to retrieve it. And, when found, the amplitude is very small. This behavior is in sharp contrast to the *summer* data that are also highly variable, but which with averaging appear to retrieve the underlying semidiurnal variation. Thus, while a similar semidiurnal tidal variation can be excited in *winter* as in *summer* and *late summer*, in propagating upward to the upper mesosphere, much happens to modify this tidal variation, to make it almost unrecognizable and to randomize it so much that the recovered amplitude is very small.

3.4. Transition Periods

The components of the wind in the October transition period, Figure 4, are clearly different from those in *late summer* and *winter*. The variation is also not simply semidiurnal. The time between the minimum in the meridional component early in the evening to the maximum later in the night is more than six hours. Working from the minimum early in the evening and assuming the variation is mostly semidiurnal, we can derive amplitudes and phases as well as the background winds. However, these are not as well determined as in *summer* and *late summer*. The meridional wind is small, but still equatorward; the background zonal wind is very close to zero. The values are given in Table 3. October winds are also clearly different from those in

November. If the November components exhibit a semidiurnal variation, then there is an approximate phase shift of five hours in going from October to November. In addition, the background meridional wind shifts from southward to weak northward, and the zonal wind increases from being near zero to being approximately 10 m/s eastward.

The March-April transition period is different from the October one. In March there is little sign of a semidiurnal variation, while one begins to appear in the April data. If it is semidiurnal, the phase is approximately one hour earlier than in the *summer*. During the nighttime observing period, the meridional component changes in March from its northward value in the *winter* months to southward and stays in that direction through October. The zonal component also makes a major transition. While eastward in both *winter* and *summer*, it is westward in both March and April. This is the only period during the year when the background zonal wind is westward. In *late summer* there is a large westward velocity for a few hours, but as described earlier, it is part of a large semidiurnal variation where the background wind is eastward. By May, the zonal wind again is eastward. The winds and the April semidiurnal tidal values are tabulated in Table 3.

4. Observational Summary and Wind Comparisons

In examining several years of the OH winds observed with a very sensitive FPI at BLO, we found three very distinct observation-based "seasons" and two transition periods, Table 2. These seasons are characterized by the estimated background winds, the semidiurnal tidal variations, and the day-to-day variability of the wind pattern. The deduced background winds and semidiurnal tides are tabulated in Table 3 and shown in Figure 9, and the daily variability is characterized in Table 4. In *late summer*, the observed winds are dominated by a very distinct semidiurnal pattern that is seen almost every day and hence in month-long averages and multiyear monthly averages. Because of its appearance in the month-long diurnal averages, this semidiurnal pattern is undoubtedly tidal in origin. Largely masked by this semidiurnal variation and subject to various assumptions discussed earlier, there appears to be a weak meridional background wind from north to south and a stronger zonal wind from west to east. In *summer*, unlike *late summer*, the observed day-to-day winds differ greatly, but an underlying semidiurnal tidal pattern again appears in month-long and multiyear monthly averages. Again, we deduce the background winds: there is a meridional wind from north to south and a zonal wind from west to east. Both components are larger than in *late summer*. In *winter*, the situation is very different. It is as if the observed pattern from day to day were almost random. In December and January we find a very weak semidiurnal pattern, but not in the other two months. We deduce the background winds for all four months: the meridional wind is reversed from the other seasons, flowing from south to north, but the zonal wind is still from west to east.

In the top panel of Figure 9, we clearly see an annual cycle in the background meridional wind and a semiannual cycle in the background zonal wind. However, the meridional wind is towards the south for twice as many months as it is towards the north. The minima in the zonal wind toward the east occur a month after each equinox, i.e., in April and October.

In the middle panel of Figure 9, we also see what appears to be a gradual 500 percent increase in the amplitude of the semidiurnal tide from *winter* to *late summer*, followed by a rapid decrease. We say "appears" because we do not have amplitudes for November, February, and March. Except for *summer*, the meridional and zonal amplitudes are nearly the same, differing by less than 5 m/s. In *summer* the difference is between 5 and 10 m/s. In *summer* and *late summer* the meridional amplitude is larger, while in December and January the zonal amplitude is larger.

In the bottom panel of Figure 9, we have essentially plotted the phase of the semidiurnal variation. Instead of displaying the maxima as a function of local solar time, we have displayed the observed minima, and a few extensions in winter, as a function of UT. This is easier to compare to Figures 4 through 8. (The local solar time of the semidiurnal variation is retrieved by subtracting 1.4 hours.) The values from Table 3 are plotted using solid black circles. In addition to these values, a few more are determined from the winds in Figure 4 by examining the minima and maxima and imposing a 12-hour period. Four such points for November and one for December are plotted as open circles. (One additional point for December and two for January do not fit on the plot.) The question that arises in examining these points is how to connect them during the winter. In going from September to November, the phase appears to move gradually earlier. An alternative interpretation, which is followed by most groups, is to show the phase shifting dramatically later. A corresponding phase shift question then arises for the spring. Rapid phase shifts during October and November and during February and March may account for the difficulty we have in finding a semidiurnal variation in these months. This will need special study at a later date.

The initial set of BLO wind data from this FPI for *late summer*, shown previously in *Rees et al.* [1990], agrees with the results presented here. They emphasized the large amplitude of the semidiurnal variation, often reaching ±50 m/s about the mean, in *late summer* and the day-to-day consistency. In contrast to this agreement, the initial set of *summer* results presented in *East et al.* [1995] does not agree with the results shown here, i.e., their averages do not show the distinct semidiurnal pattern. This difference arises, most likely, because the *summer* data are highly variable and more days were included in the present work than previously. We could do so because we used a more sophisticated cloud detection scheme. For instance, we did not reject nighttime data because clouds were visible during the preceding daytime. (Daytime clouds very often dissipate after sunset.) We also had available more years of summer data. In this sense, the *East et al.* [1995] work serves to emphasize the great day-to-day variability in the summer data and the need for extensive observations.

While we have given estimates of the semidiurnal tide and of the background winds, it is very difficult to do so with observations that vary in length from 6 to 11 hours. Furthermore, it is beyond the scope of this paper to perform and present a spectral analysis of the type discussed by *Crary and Forbes* [1983] and used on averaged O_2 intensity and temperature data from BLO by *Wiens et al.* [1995], or of the type based on simultaneous fits to all the good days in a month, as was used by *Niciejewski and Killeen* [1996] on OH and O(^{1}S) wind data from Peach Mountain Observatory (PMO). Instead of performing one of these spectral analyses, we present arguments in Section 3 about (1) an apparent 12-hour period (or 6-hour half period) in the wind variations, (2) the meridional component leading the zonal component by three hours (phase quadrature for a 12-hour wave), and (3) similar amplitudes for meridional and zonal components. Taken together, these arguments suggest the dominance of a semidiurnal tide between April and October and the existence of such a tide in December and January. This dominance is supported by the results from *Niciejewski and Killeen* [1996] in which they could not improve on the harmonic fit to the winds by including a diurnal variation or variations of higher frequency than semidiurnal. In partial contrast, MF and meteor wind radar results show the existence of diurnal in addition to semidiurnal variations [e.g., *Manson et al.*, 1989; *Franke and Thorsen*, 1993]. However, the diurnal component is almost always much smaller. Hence our assumption that the amplitude of a diurnal tide is small compared to the background winds—an assumption needed to find the background wind—is reasonable. This is much the same approach as taken by *Fleming et al.* [1996] with HRDI data from UARS to find the background winds from daytime data in this altitude region.

It is instructive to compare our background winds to those from other sources. The zonal wind is available at 87 km and 50° N from HRDI [*Fleming et al.*, 1996], as just mentioned. It is derived from daytime data by assuming no diurnal tide. They show eastward winds all year long with the exception of a near-zero speed in March and a small westward speed in April. These results, including the April reversal, are qualitatively similar to ours. However, they differ quantitatively, particularly in *winter*. In December HRDI shows an eastward wind of up to 30 m/s, whereas we show an eastward wind of 5 m/s. Three possibilities exist: the difference may arise, in part, because of an 8° latitude difference between BLO and the latitude for which the HRDI data were presented; the difference may indicate the existence of a large diurnal tide with its maximum near noon; or the difference may be real (e.g., the HRDI results represent a longitudinal mean, whereas ours are local). Presumably, the HRDI data could be displayed for

42° N to examine the latitudinal dependence. Information about the diurnal tide is available from radar observations. However, the radar results are not conclusive. The results from Durham [*Manson et al.*, 1989] show December amplitudes between 5 and 15 m/s with a phase between 0800 and 1000 LT. However, the radars at Garchy, Monpazier, Saskatoon [*Manson et al.*, 1989], and Urbana [*Franke and Thorsen*, 1993] show smaller amplitudes of approximately 5 m/s and a phase maximum in the late afternoon or evening. Thus, at the moment we cannot reconcile the magnitudes of our zonal winds from BLO with the mid-winter HRDI data from UARS.

A similar difference exists between our zonal winds and HRDI's in October. We find a background zonal wind that is essentially zero, whereas the HRDI wind is greater than 20 m/s towards the east. The same set of three possibilities exists for reconciling the two observations, as given above. However, the diurnal tide seems more likely as an explanation in this case. The radars show a diurnal component with a maximum amplitude between 5 and 10 m/s occurring in the early afternoon [*Manson et al.*, 1989; *Franke and Thorsen*, 1993]. This would have the effect of increasing the eastward wind during the daytime and suppressing it during the nighttime. In addition, the difference between the HRDI and FPI winds are in the same direction as found in other comparisons [*Burrage et al.*, 1996].

Another data set with which to compare is from a 15-month campaign at Peach Mountain Observatory [*Niciejewski and Killeen*, 1996], also at mid-latitudes, that included OH wind observations. They performed a spectral analysis, as mentioned above, and found that the best least squares fit was obtained with just the background wind and the semidiurnal variation. Thus their work supports our ignoring a diurnal tide, or else their spectral analysis was not sensitive to it. They found a similar behavior to ours for the background wind: they found the winds weakly towards the south between mid March and mid October, weakly towards the north the rest of the time, towards the east all year long with the strongest eastward winds in July and August. They did not observe the westward directed wind that we did in March and that we and HRDI did in April, and they did not observe the strong zonal winds we did in June. They, too, found the largest-amplitude, semidiurnal variations in August and September. Their phases agreed with ours to better than 1.5 hours. Unlike our results, they found a second period of large-amplitude, semidiurnal variations in March and April. Also, unlike our results, they found approximately the same amplitudes in winter as in summer. These are significant differences between the two sites.

Historically, the wind climatology in the upper mesosphere has been determined with meteor wind, medium-to-low frequency, and MST radars. Climatologies from several mid-latitude sites (43–52° N and S) have been reported by *Manson et al.* [1989] and the climatology from an MF radar near Urbana has been reported by *Franke and Thorsen* [1993]. To first order, these climatologies are similar to ours, but significant differences occur. For instance, compared to our FPI data, the radar data in *late summer* show a much smaller semidiurnal variation and in *winter* show a much larger semidiurnal variation. The winter amplitudes at Saskatoon, Garchy, and Monpazier are larger than the summer ones [*Manson et al.*, 1989], whereas at Durham and Christchurch [*Manson et al.*, 1989] and at Urbana [*Franke and Thorsen,* 1993] they are equal to the summer ones. Compared to our FPI data, the radar data from Saskatoon and Durham [*Manson et al.*, 1989] and from Urbana [*Franke and Thorsen*, 1993] show very good phase agreement between April and September, i.e., mostly within an hour. In December and January, the Durham and Urbana phases agree with ours within 1.5 hours. In October, November, February, and March when we had trouble determining a semidiurnal amplitude and phase, these radar sites show considerable scatter in their phases. A detailed comparison of the BLO and radar winds from the vicinity of 87 km would be very useful, but is beyond the scope of this paper. Nonetheless, the basic agreement of these climatologies is important. Because the Fabry-Perot technique is totally independent of the radar technique, the basic agreement provides a strong confirmation of the large body of radar wind data. The basic agreement also supports the assumption that the OH observations do provide a good measure of what is happening in the immediate vicinity of 87 km.

In addition to these observations, much theoretical work has been carried out covering the diurnal and semidiurnal tides. The latest efforts are incorporated into the global-scale wave model (GSWM) [*Hagan et al.,* 1995]. The GSWM results for 42°N and 86 km are given in Table 5 for the four months for which they are available. The speeds are positive to the geographic east and north. The phases are given in LST, in hours, for the maximum positive speed. The semidiurnal variations can be compared to the semidiurnal climatology deduced from our observations, given in Table 3.

The GSWM semidiurnal results show good phase quadrature with the meridional component leading the zonal and essentially equal amplitude components, more so than in our observations. In January, the model shows a large amplitude semidiurnal tide, whereas we show a weaker one. In April, July, and October the model amplitudes are smaller than what we deduce from the observations by factors of three, six, and two, respectively. In July, the observed and modeled phases are within half an hour of each other, which represents excellent agreement. In April they are within approximately two hours of each other, with the observed phase leading the model phase. In January, the observed phase leads the model one by approximately three hours. By October, the observed and modeled phases differ by four hours with the model phase leading the observed phase. While the observed phase moves three hours earlier from July to October, the modeled phase moves seven hours earlier or five hours later. This is a major phase difference. Unfortunately, model estimates are not available for late summer when our observed semidiurnal variation is largest.

Thus we have major differences between the modeled semidiurnal variations and our determinations from the observations. The relative amplitudes differ considerably. During January the observed amplitude is approximately 60 percent of the model value, whereas during the rest of the year the observed amplitudes are two to six times larger than the model values. The relative phases also differ considerably. The observed and model phases agree very well in July, but differ by approximately two hours in April and three in January, and by four hours in the opposite direction in October. The semidiurnal variations so dominate the FPI observations during most of the year and the differences between observed and model amplitudes and phases are so large that even a full spectral analysis of the observations would be unlikely to change these differences.

The diurnal tidal variations are included in Table 5 as a reminder that we are ignoring this term in deriving the background wind and semidiurnal tide. However, in view of the differences between observed and model semidiurnal variations, it is premature to use these model results to try to improve the derived values.

5. Discussion

The wind climatology that we observe at 87 km is, as discussed in the introduction, the consequence of many radiative, chemical, and dynamical processes that occur throughout the middle atmosphere. Beyond the local absorption of solar energy, these include the excitation of gravity waves, tides, and planetary waves lower in the atmosphere; the filtering, interaction, transmission, and breaking of these waves in the passage to the upper mesosphere; and the deposition of momentum and production of turbulence in the region above where breaking or saturation begins. Because our climatology and its variability are the combined result of all these processes, they reflect the important processes happening at lower altitudes. To account for our observed climatology, we examine the effects of many of these processes in the rest of this section. In so doing we refer to model calculations [e.g., *Holton,* 1983; *Geller,* 1983; *Garcia and Solomon*, 1985] and other observations. The results of these discussions are summarized in Table 6 in the next section

5.1. Winds at 87 km

In our climatology, Figure 4 and Table 3, the zonal wind is toward the east almost all year long, indicating that the 87-km altitude of the OH emission is above the mesospheric jets [e.g., as shown in *Fleming et al.*, 1996, for HRDI and two model atmospheres]. Surprisingly, the speed is greater during most of the *summer* and *late summer* than during the *winter*. Compared to radiative-equilibrium solutions for the winds, the deduced eastward speed is greatly reduced in *winter*, while in *summer* and *late summer* the wind direction is reversed from westward and the air accelerated to a greater eastward speed than in *winter*. The significant exception to the eastward zonal wind is in March and April when the wind is westward. This timing appears to coincide with the development of the westward jet centered at approximately 65 km, i.e., the mesospheric jet. Otherwise, in March and October—essentially at the equinoxes—the observed background zonal wind appears to be nearly zero. While the near-zero velocity in March appears to coincide with the reversal of the mesospheric jet from eastward to westward at lower altitudes, the near zero velocity in October is approximately a month after the reversal back to eastward.

The meridional wind is toward the north in *winter* and toward the south in *summer* and *late summer*, with the speed being greater in *summer* (10 m/s) than in *winter* (7 m/s). The meridional wind appears to change direction very close to spring equinox and a month after fall equinox. This basic summer-to-winter flow is what is expected from dynamical-radiative models to account for the cold summer mesopause and the warm winter mesopause [e.g., *Holton*, 1983; *Garcia and Solomon*, 1985]. The zonal wind reversal in *summer* is also consistent with the stronger meridional flow in *summer* than in *winter*.

Qualitatively, the observed behavior is consistent with predictions based on the *Lindzen* [1981] gravity wave parameterization of wave drag and eddy diffusion, which give rise to the mesospheric jets centered near 65 km and their closing at higher altitudes [e.g., *Holton*, 1983; *Garcia and Solomon*, 1985]. That the jets are closed at 87 km indicates that the gravity wave effects there are greater than at lower altitudes. Furthermore, the reversal of the zonal wind in summer compared to "just" the slowing down of the wind in winter indicates a seasonal dependence of the gravity wave populations. In summer, the gravity waves have to have an eastward phase velocity to reverse the winds. This is consistent with critical layer interactions whereby gravity waves with a small eastward phase velocity would be filtered out by the eastward jet stream, or tropospheric jet, those with a westward phase velocity would be filtered out by the westward mesospheric jet, and those with a near zero phase velocity would be filtered out near 20 km in the stratosphere where the wind profile passes through zero between the tropospheric and mesospheric jets. The only zonally propagating gravity waves not to be filtered out by the background winds would be those with an eastward phase velocity larger than the eastward jet stream. They would continue upwards and break (or reach saturation) over a range of altitudes in the mesosphere and lower thermosphere giving up both momentum and energy.

If the generation of gravity waves were isotropic and their filtering were seasonally symmetric, then in winter we would expect to see westward zonal winds at 87 km. However, with the exception of March and April, we observe only eastward winds in the climatology. This implies there is no significant population of gravity waves with a westward phase velocity that reaches the vicinity of 87 km. However, with both the tropospheric and mesospheric jets directed eastward, gravity waves with a westward phase velocity, if they were generated, would not be filtered out. This suggests that such gravity waves are not generated nearly as readily as those with an eastward phase velocity in summer. However, we also know from temperature observations that the situation in the stratosphere and mesosphere is much more complicated in winter than in summer as a result of planetary waves, stratospheric warmings, and mesospheric inversion layers [e.g., *Hauchecorne and Chanin*, 1983; *Hauchecorne et al.*, 1987; *Wickwar et al.*, 1997a]. Unfortunately, there are no extensive wind observations in this altitude region. Until they can be made, we have to assume that various possibilities may exist for critical-layer interactions with dynamical features besides the background winds or that they may exist for wave-wave interactions. Thus because gravity waves with a westward phase velocity are either not generated or are filtered out, they do not have as large an impact on the circulation at 87 km in winter as gravity waves with an eastward phase velocity have in summer.

The difference between gravity waves with an eastward phase velocity reaching 87 km in summer, but not those with a westward phase velocity in winter, is supported by the OH gravity wave climatology observed at PMO [*Wu and Killeen*, 1996] with a CCD all-sky camera. They could detect gravity waves producing a 7.5 percent modulation of the OH emission. They observed monochromatic gravity waves on 68 percent of the nights in *summer,* 6 percent in *late summer,* 9 percent in the spring transition period, and far less than 1 percent in the *winter* and the October transition period. These waves had a zonal component of phase velocity toward the east on at least 70 percent of the observations. The idea of eastward propagating gravity waves passing through 87 km and breaking at higher altitudes in *summer* is also supported by the HRDI observations of the peak of a strong eastward jet centered near 97 km [*Fleming et al.,* 1996]. Although the wind does turn towards the west at higher altitudes in *winter*, there is no corresponding strong westward jet. This does suggest that a weak flux of westward propagating gravity waves reaches 87 km and above. However, the lower speed indicates a much weaker flux than for the eastward propagating gravity waves.

While few gravity waves with a westward phase velocity may reach 87 km in *winter*, the observed eastward winds are nonetheless very small, implying that gravity waves with a phase velocity less than that of the eastward zonal wind are giving up momentum and energy at that altitude to decelerate the wind. A likely population of gravity waves is the one with essentially zero phase velocity, whose excitation is attributed to winds at essentially mountain-top level. Such winds exist. While the flow is highly variable because of changing meteorological conditions, it does have an annual cycle that shows up in a climatology, which can be determined from radiosonde data acquired daily over the western states. In Figure 10 we show the annual variation of the geostrophic wind speed at 700 mbar (approximately 3 km), interpolated to the region over BLO, determined from 30 years of data [*Westbrook,* 1980]. There is a strong annual variation with the maximum speeds, hence gravity-wave forcing, in *winter* and the minimum speeds in *summer* and *late summer.*

At least with respect to the background winds, which are all eastward in *winter*, gravity waves with a zero-phase velocity would not experience a critical layer interaction in propagating up to 87 km. However, because of the reduced phase velocity they will break at lower altitudes than gravity waves with strong westward or eastward phase velocities [e.g., *Holton* 1983; *Garcia and Solomon*, 1985]. This would greatly reduce the likelihood of a monochromatic gravity wave reaching 87 km in winter, which is consistent with the PMO observations of no gravity waves in winter at their 7.5 percent modulation threshold. It is consistent with the HRDI observations that there is no strong westward jet in winter between 95 and 105 km in contrast to the strong eastward jet in summer. Such a jet would require westward propagating gravity waves, some of which would break above 87 km.

Direct observations of gravity wave energy and deduced values of the divergence of the horizontal momentum flux support both winter and summer maxima of gravity wave activity in the upper mesosphere. Potential energy densities calculated from lidar observations at Haute Provence (44° N) and Aberystwyth (52° N) show a systematic change with altitude from a winter maximum in the stratosphere to both winter and summer maxima in the middle mesosphere [*Wilson et al.*, 1991; *Mitchell et al.*, 1991]. The wind variance observed with the MF radar at Adelaide (35° S) at 86 km [*Vincent and Fritts*, 1987] showed this. Kinetic energy densities deduced from MU radar observations (35° N) show a larger summer maximum than winter maximum [*Tsuda et al.*, 1990]. Flux divergences from radar observations at Adelaide and Shigaraki (the MU radar) also show maxima in the upper mesosphere at the two solstices [*Reid and Vincent*, 1987; *Tsuda et al.*, 1990].

A final point about the background winds in *winter* is their great variability, which was shown in Figure 8. Very often, this background wind is relatively constant for a whole night. This constancy suggests that it is not tidal in origin: it is perhaps related to planetary waves, which have much larger periods and are slowly moving in longitude. This background wind can also be very large. The HRDI results shown in Figure 1 of *Smith* [1996] of a planetary-scale wind structure have the proper characteristic to explain our observations.

5.2. Semidiurnal Tides at 87 km

Returning to the climatology, Figure 4 and Table 3, the most dramatic aspect of the OH wind observations at BLO is the very strong semidiurnal variation in *late summer*. This is clearly a manifestation of the semidiurnal tide that is excited in the troposphere and stratosphere by the absorption of solar radiation in H_2O and O_3, respectively. The semidiurnal variation appears on most nights and is characterized by an amplitude of approximately 30–50 m/s for both components, with the meridional component leading the zonal component by approximately 3 hours. However, there is a half hour to an hour of phase jitter from night to night. On the remaining nights, the pattern changes considerably, as opposed to having a semidiurnal variation with a much smaller amplitude. This implies that something major happens to the semidiurnal oscillation as the tide propagates upwards on those nights. A consequence of the phase jitter and the other temporal patterns is that the amplitude of the semidiurnal variation in the climatology is reduced to approximately 25 m/s. Adding six hours to the observed climatological velocity minima to the north and east, the local solar times of the meridional and zonal phases are approximately 0336 and 0612.

In *summer*, unlike *late summer*, the semidiurnal variation does not stand out on most of the observed nights. However, it does appear on a few nights. When it appears, it has approximately the same amplitude as in *late summer*. On the other nights, the temporal pattern is very different. This implies, again, that there are significant night-to-night changes to the propagation conditions for the semidiurnal tide. Nonetheless, when enough nights are averaged, the semidiurnal pattern appears. The amplitude of the semidiurnal variation of the meridional component is approximately 60 percent greater than the zonal components in the climatology, but roughly half to 75 percent of what they are in *late summer*. The phase maxima occur approximately an hour later than in *late summer*, with the meridional component again leading the zonal component by approximately 3 hours.

In *winter*, the situation is more extreme. As in *summer*, the semidiurnal variation does not stand out in the observations of individual nights. Yet, a semidiurnal variation with the usual large amplitude does appear on a few nights. However, unlike *summer*, it takes considerable averaging to obtain a weak semidiurnal variation in part of the winter climatology. For some months and years, a possible semidiurnal variation emerges with an amplitude of approximately 5 m/s. But, the phase quadrature apparent in the other seasons is missing and the phase can appear to change by many hours from one year to the next. This most likely reflects considerable month-to-month and year-to-year variability. A consequence of this is that it took four years of data to determine a semidiurnal pattern in half of the winter months. The upward transmission of the semidiurnal variations is more greatly affected in winter than in the other seasons and, whatever the mechanism, it appears to occur randomly in time.

Because of the almost nightly occurrence of a strong semidiurnal variation in what we have called *late summer*, which is close to fall equinox, it is natural to look for a similar variation near spring equinox. But as is apparent in Figure 4 and Table 3, the two equinox periods are very different. There is a major fall-spring asymmetry.

Thus the observations show considerable variation in the semidiurnal tide from season to season. While details of the tidal excitation should vary during the year (e.g., the amounts of H_2O and O_3, and the number of hours of sunlight), to first order the tidal excitation should be very similar every day. For instance, the amplitude of the tidal excitation in going from *summer* to *late summer* should not increase by a factor of almost two. This assumption of the day-to-day similarity is borne out, as we have already indicated, in the semidiurnal variation observed on individual nights, i.e., in *summer* and *winter* the nights with a semidiurnal variation have amplitudes similar to the days in *late summer*. This suggests that the great variety in temporal patterns seen at 87 km from night to night, and hence the major seasonal variation of the tidal amplitude in the climatology, has to arise from variations in the transmission of the tide through the atmosphere above the altitude of generation.

In *late summer* the tidal oscillations on most days are able to propagate with little interference or interaction, growing exponentially up to at least 87 km. However, an indication of interference during the transmission and growth does appear in that they suffer small phase shifts from night to night and the temporal pattern is very different on a few nights. Sufficient interference occurs that the semidiurnal amplitude in the climatology is approximately 60 percent of what it is on some individual nights. Because *late summer* is centered on the reversal of the mesospheric jet—approximately 1 September [*Fleming et al.,* 1996]—a possible explanation is an interaction between the tidal oscillation and the mean wind. However, this explanation is negated by the absence of a strong semidiurnal variation at 87 km in March and April at the time of the other reversal of the mesospheric jet. Thus the transmission effects on the semidiurnal tide do not appear to be simply the consequence of interactions between the semidiurnal tide and the background wind.

Another possible source of interference to the transmission of the semidiurnal tide through the middle atmosphere is gravity waves [e.g., *Fritts and Vincent,* 1987; *Wang and Fritts,* 1991; *Miyahara and Forbes*, 1992]. As already mentioned, several groups have found maxima in gravity wave activity in summer and winter. In the stratosphere and lower mesosphere, a single maximum in gravity wave potential energy, based on either density or temperature fluctuations, is seen in winter [e.g., *Wilson et al.*, 1991; *Mitchell et al.*, 1991; *Marsh et al.*, 1991; *Murayama et al.*, 1994b; *Whiteway and Carswell*, 1995], whereas higher in the mesosphere a summer maximum also occurs [*Wilson et al.*, 1991; *Mitchell et al.*, 1991], and near the summer mesopause the gravity-wave kinetic energy shows a main summer maximum and a smaller winter maximum [*Tsuda et al.*, 1990, 1994]. This change with altitude from an annual to a semiannual pattern is consistent with the previously discussed critical-layer filtering that gives rise to the preferential transmission of gravity waves with a near-zero phase velocity in winter, and gravity waves with an eastward phase velocity in summer. As deduced from lidar-derived altitude profiles of potential energy [*Wilson et al.*, 1991; *Mitchell et al.*, 1991; *Whiteway and Carswell*, 1995], winter gravity waves break starting in the upper stratosphere, and summer gravity waves break starting near the stratopause. That the gravity waves break at a lower altitude in winter than in summer leads to a greater altitude range in winter for interaction with tidal oscillations. In addition, the lidar studies cited above and *Thomas and McDonald* [1997] find that the gravity-wave potential energy in the stratosphere in winter is up to an order of magnitude greater than in summer. Thus the summer-winter differences in the appearance of the semidiurnal tide at 87 km appear to be consistent with the interaction of the tide with gravity waves. However, the one caveat is that the winter stratosphere and mesosphere have many complex variations because of planetary waves, stratospheric warmings, and inversion layers that might give rise to additional interactions with the tidal variations.

But what about the much stronger semidiurnal tide seen at 87 km in *late summer* than in *summer* and *winter,* and the fall-spring asymmetry? *Murayama et al.* [1994a], using the MU radar, found a strong correlation between the speed of the jet stream near 13 km and gravity wave activity in the lower stratosphere. Both showed a maximum in winter and a minimum in August, with a large fall-spring asymmetry. To explain fall-spring asymmetries in other parameters in the upper mesosphere, at higher latitudes, *Luo et al.* [1995] had to reduce the gravity-wave source in the August-September time frame to introduce a rapid cessation of gravity wave forcing in their model calculations. As shown by the winds speeds just above the mountains in northern Utah, Figure 10, there will also be a *summer* minimum in the topographic forcing of gravity waves, with the forcing in *late summer* remaining very low. These three independent "observations" taken together strongly support a minimum in gravity wave activity in *late summer.* Such a minimum in *late summer* gravity-wave activity combined with our observed large semidiurnal tides at 87 km is consistent with, and therefore supports, the idea that gravity waves do interact with the semidiurnal tide to affect its upwards propagation. Because both the topographical source of zero-phase speed and the jet-stream source of, at least, eastward-phase speed gravity waves are minimized, the gravity wave activity in the mesosphere will remain low compared to winter and summer whatever the direction of the mesospheric jet.

6. Conclusions

As demonstrated by the observations shown in this paper, the imaging Fabry-Perot interferometer that we are using at BLO is a very sensitive instrument for the study of the OH winds. We have examined four years of observations to develop a climatology of the mid-latitude winds near 87 km, Figure 4. In addition to providing excellent data for finding monthly climatologies, the great sensitivity of the FPI enables it to provide excellent wind observations with good time resolution during individual nights. We have used these extensive wind observations and the variability of these winds to identify three very distinct seasons and two transition periods. They consist of a four-month *winter*, a three-month *summer*, and a two month *late summer*, with transition periods on either side of *winter*. The months belonging to each season are given in Table 2 and the observations are summarized in Tables 3, 4, and 6, and Figure 9, and discussed in Section 4. In addition to these overall summaries for the entire period, annual climatologies show distinct interannual variation in both *summer* and *late summer*.

The climatology is so dominated by a semidiurnal variation in all seasons except *winter* that we are able to determine the background winds, provided the amplitude of the diurnal tide is small compared to the background wind. These winds are summarized in Tables 3 and 6. The zonal wind is directed towards the east, except in March and April, and the meridional wind is directed from summer to winter. The equatorward flow is stronger in *summer* than the poleward flow in *winter*, and the eastward zonal flow is stronger in *summer* than in *winter*. We also determined the semidiurnal tidal variability. The amplitudes and phases are given in Tables 3 and 6. This tidal variation is extremely large in *late summer*, large in *summer*, and extremely small in *winter*. The meridional component is bigger than the zonal component, except in winter, and the two components are in approximate phase quadrature with the meridional component leading the zonal by three hours.

These observations have been compared to others at 87 km and to model calculations for the same altitude. Our first comparison with UARS is with the zonal winds from the HRDI instrument. There is qualitative agreement in that both instruments show an eastward wind all year long, except for March and April, when it is westward. However, the HRDI eastward winds appear to be significantly faster than ours. This might occur because they have daytime observations, while we have nighttime observations, and both groups have to ignore diurnal tides to find the winds. It might also occur because of a latitude difference between the two data sets. It will be useful to make a more direct comparison with nighttime OH winds from WINDII when they become available.

We appear to have good agreement with MF radar observations and with more limited OH observations at PMO. The overall good agreement with the MF radar winds—both amplitudes and phases—is a strong confirmation of those results, because we are using a totally different technique. Conversely, the overall good agreement also validates our FPI results. However, within this agreement, some differences appear such as the radar winds showing stronger semidiurnal variations than we do in *winter*, but smaller ones in *late summer*. Similarly the PMO FPI shows stronger semidiurnal variations in winter than we do, and has a strong relative maximum at spring equinox while we do not.

A consistent difference in these comparisons with observations from other sites is the near absence of a semidiurnal tide over BLO in winter. This is the time period when topographically generated gravity waves will have the largest impact on the stratosphere and mesosphere, and when the low-altitude winds are strongest. It thus appears that the Rocky Mountains have a significant impact on the wave fields and, by extension, an integrated effect on the general circulation.

Very importantly, the seasonal behavior of our deduced meridional and zonal winds is consistent with model calculations of what is needed to account for cold summer temperatures and warm winter temperatures in the upper mesosphere. This, in turn, supports the very significant role of gravity waves in the model parameterization.

We have both significant agreements and disagreements when we compare our semidiurnal tidal variations with those calculated by the GSWM model for four months. The model has a significant tidal amplitude in January, whereas we have a much weaker one. Otherwise, the observed tidal amplitudes are much greater—factors of two to six—than the calculated ones. The tidal phases agree very well in July, differ by two hours in April and three hours in January, and differ by four hours in the opposite direction in October. The amplitudes and the October phase difference are particularly significant failings. It appears that somehow the semidiurnal tide is not being treated correctly. Perhaps, in the model, the Rocky Mountain topographical source of gravity waves is not included in winter. Perhaps, in the model, the semidiurnal tidal source is not great enough or the tides are being damped too much in transmission through the middle atmosphere to 87 km. It would be useful to make a more extensive comparison when we have a good spectral analysis of the FPI data and the corresponding GSWM results are available for all months. Nonetheless, in light of the GSWM being the state-of-the-art model, in that it attempts to include every known process, the differences we have already found in amplitudes and phases raise an important question. Namely, the model tidal results are obtained using averaged inputs. In contrast, the climatological results are an average of wind fields determined from highly variable inputs. If the system were linear and the model included all significant inputs, then the model and observed tides should agree reasonably well. Does their apparent disagreement indicate that non-linear processes are more important than previously thought?

The deduced semidiurnal tides at 87 km were shown to depend greatly on the daily variability of the observed winds, e.g., in *late summer* a strong tide was found when almost every day had a strong semidiurnal wind variation, whereas in *winter* a very weak tide was found when every day had a very different temporal variation. Although there is substantial seasonal variation, the tidal excitation should not vary greatly from day to day. Consequently, the observed variability at 87 km must reflect variability in the transmission or passage of the tidal oscillations through the middle atmosphere. The strong fall-spring asymmetry in the tidal amplitudes rules out the much more symmetric background wind, in particular the mesospheric jet, as the major factor affecting the tidal transmission. Instead, it focuses attention on the possible role of gravity waves in affecting the tidal transmission.

Thus in examining the background winds and semidiurnal tides, it appears that both are greatly affected by gravity waves. Most encouragingly, these two very different aspects of the wind field appear to depend on the same, seasonally different gravity-wave populations. A consistent picture begins to emerge that ties together many of the major features. In *winter*, the strong, but highly variable, prevailing winds over the Rockies give rise to a strong topographical source of gravity waves with near-zero phase speed. With eastward winds in the tropospheric and mesospheric jets, these gravity waves can propagate upward without a critical-layer interaction, and start to break or saturate in the stratosphere. In the mesosphere, these breaking gravity waves will decelerate the mesospheric jet and adversely affect the upward propagation of the semidiurnal tide. In the vicinity of 87 km they will continue to decelerate the eastward wind but cannot reverse it. The saturation process occurring throughout the mesosphere will cause enough cascading in energy that few monochromatic gravity waves will be left to excite detectable airglow intensity variations at 87 km.

In *summer*, a very different situation exists. While there is still a prevailing wind over the Rockies, the resulting gravity waves with a near zero phase velocity will experience a critical-layer interaction in the stratosphere as the prevailing winds at these higher altitudes shift from eastward in the tropospheric jet to westward in the mesospheric jet. The tropospheric jet stream, or wind gradients associated with it, then becomes the major source of gravity waves. Those leaving the vicinity of the jet stream with an eastward phase velocity can propagate upward throughout most of the mesosphere without a critical-layer interaction. However, those with a westward phase velocity, if any, will experience a critical-layer interaction with the westward mesospheric jet. These gravity waves with an eastward phase velocity break at a higher altitude than the zero-phase velocity gravity waves in winter. In the mesosphere they will decelerate the westward jet and by 87 km they will reverse the wind direction and give rise to an eastward jet in the lower thermosphere. Because the onset of saturation for these gravity waves occurs at a higher altitude than for the zero-phase speed waves in *winter*, there is a smaller range of altitudes for them to interact with and disrupt the semidiurnal tide below 87km, and more monochromatic waves will survive to excite detectable airglow intensity variations at 87 km.

In *late summer* the jet-stream source of gravity waves is weak compared to the *summer* and the topographical source is weak compared to the *winter*. Irrespective of where critical-layer filtering occurs, which will be changing during this period as the mesospheric jet shifts from westward to eastward, and back and forth several times, the gravity wave sources are weak. A major consequence is that the semidiurnal tide will propagate upwards to 87 km with minimum interference. Some detectable airglow variations will also occur at 87 km from eastward propagating gravity waves that reach that altitude without breaking.

The spring equinox period differs from *late summer* in that both the jet-stream and topographical sources of gravity waves are stronger. This leads to an increased disruption of the upward propagating semidiurnal tide and the smaller observed tide at 87 km.

Thus we have been able to account for much of the observed and reported behavior by relying on two gravity-wave populations: one with a near-zero phase velocity that dominates in *winter*, and one with an eastward phase velocity in *summer*. The former is most likely associated with the topographic generation of gravity waves, the latter with the jet stream.

Because a climatology, like the one reported here, is so heavily averaged, it would be difficult to detect the expected strong impact of individual convective storms as a gravity-wave source. The detection of that source is probably best done with case studies. Another question that arises from our observations and other middle-atmosphere observations is what happens to gravity waves with a westward phase speed? From the picture presented here, they could propagate upward in winter past the eastward tropospheric and mesospheric jets without a critical-layer interaction. However, their existence is not manifested in the winter gravity wave activity in the upper mesosphere, the significant detection of airglow variations at 87 km, or a reversal of the winds to westward in the lower thermosphere. One possibility is that the jet-stream source is anisotropic, preferably producing gravity waves with an eastward phase speed. Another possibility is that our picture of what happens in the mesosphere in winter may be too simple. It is hard to believe that the very large, unexplained temperature fluctuations or inversion layers in the winter mesosphere are not accompanied by strong dynamical features that might give rise to critical-layer interactions in this region. This is an area where extensive new observations are needed.

The observations, discussions, and conclusions are summarized in Table 6. Our observations are in bold. Other information about the middle atmosphere that is needed to account for the observations is given in a regular font. Taken together, this table attempts to give an integrated picture of much of what is happening in the mid-latitude, middle atmosphere.

A final comment is on the importance of having long-term sets of observations. We earlier mentioned how an early and limited FPI data sample in one season gave rise to the wrong conclusion about the climatology for that season. We have also seen the great variability or "weather" in much of the data, particularly in winter, which requires considerable averaging to find the mean behavior. By having multiple years of data available, we were able to confirm such important features as the large-amplitude semidiurnal tide in *late summer* compared to the much smaller tide in the vicinity of spring equinox. To attempt to understand our observations, it was important to have the results from other long-term sets of observations—MF and VHF radars, Rayleigh-scatter lidars, airglow imagers—that covered other portions of the middle atmosphere and other parameters. Given the climatology and the model summarized in Table 6, we now have a framework for examining the intensities and the temperatures, comparing subsets of the data (e.g., the interannual variations), making detailed comparisons of the FPI winds to other winds such as those from the MF radars and the HWM-93 [*Hedin et al.*, 1996], comparing the FPI results to essentially co-located Rayleigh-scatter lidar temperatures from throughout the mesosphere, and comparing the FPI results to the prevailing winds over the Rockies. However, such studies require adequate resources for all four essential aspects of the work: continued development and operation of high-performance instrumentation, adequate maintenance of the instrumentation and observatory facilities, preparation and execution of the primary data reduction, and detailed analysis of the data and associated intercomparisons with models and other available data.

Acknowledgments. This work was made possible by significant contributions to the Fabry-Perot interferometer and the Bear Lake Observatory by Utah State University, by NSF CEDAR grants from the Upper Atmospheric Facilities Program in the Division of Atmospheric Sciences and by a NASA grant for correlative measurements in support of UARS. The analysis was supported, in part, by NSF CEDAR grant ATM-9302354. One of the co-authors (Maj. Vadnais) was supported by the Air Force Institute of Technology while at USU pursuing her M.S. We thank Laura Murphy, John Maloney, and Michael Howsden of USU for contributions to this work. We thank Maj. Kenneth C. Beissner of the USAF and Dr. Thomas D. Wilkerson of USU for scientific discussions and critically reading the manuscript. We also thank Dr. Maura Hagan of NCAR and the CEDAR data base for providing the tidal calculations from the GSWM, and Prof. Don Jensen of USU for information on the prevailing winds over the Rockies.

References

Alexander, M.J., A simulated spectrum of convectively generated gravity waves: Propagation from the tropopause to the mesopause and effects on the middle atmosphere., *J. Geophys. Res.*, *101*, 1571–1588, 1996.

Alexander, M.J., J.R. Holton, and D.R. Durran, The gravity wave response above deep convection in a squall line simulation, *J. Atmos. Sci.*, *51*, 2212–2226, 1995.

Bacmeister, J.T., Mountain-wave drag in the stratosphere and mesosphere inferred from observed winds and a simple mountain-wave parameterization scheme, *J. Atmos. Sci.*, *46*, 377–399, 1993.

Baker, D.J., and A.T. Stair, Jr., Rocket measurements of the altitude distributions of the hydroxyl airglow, *Phys. Scripta*, *37*, 611–622, 1988.

Burrage, M.D., W.R. Skinner, D.A. Gell, P.B. Hays, A.R. Marshall, D.A. Ortland, A.H. Manson, S.J. Franke, D.C. Fritts, P. Hoffman, C. McLandress, R. Niciejewski, F.J. Schmidlin, G.G. Shepherd, W. Singer, T. Tsuda, and R.A. Vincent, Validation of mesosphere and lower thermosphere winds from the high resolution Doppler imager on UARS, *J. Geophys. Res.*, *101*, 10365–10392, 1996.

Chanin, M.-L., N. Smires, and A. Hauchecorne, Long-term variation of the temperature of the middle atmosphere at mid latitude: Dynamical and radiative causes, *J. Geophys. Res.*, *92*, 10933–10941, 1987.

Choi, G.H., I.K. Monson, V.B. Wickwar, and D. Rees, Seasonal and diurnal variations of temperature near the mesopause from Fabry-Perot interferometer observations of OH Meinel emissions, *Adv. Space. Res.*, in press, 1997a.

Choi, G.H., I.K. Monson, V.B. Wickwar, and D. Rees, Seasonal variations of temperature near the mesopause from Fabry-Perot interferometer observations of OH Meinel emissions, *Adv. Space Res.*, in press, 1997b.

Collins, S.C., T.D. Wilkerson, V.B. Wickwar, J.C. Walling, D.F. Heller, and D. Rees, The alexandrite ring laser: A spectrally narrow lidar light source for atmospheric fluorescence and absorption observations, in *Advances in Atmospheric Remote Sensing with Lidar*, Ed. by A. Ansmann, R. Neuber, P. Rairoux, and U. Wandinger, 577–580, Springer Verlag, Berlin, 1997.

Crary, D.J., and J.M. Forbes, On the extraction of tidal information from measurements covering a fraction of a day, *Geophys. Res. Lett.*, *10*, 580–582, 1983.

East, S.A., N.P. Meredith, M.J. Harris, D. Rees, V.B. Wickwar, I.K. Monson, and H.G. Muller, First summer results on winds in the upper mesosphere derived from the 843 nm hydroxyl emissions measured from the Bear Lake Observatory, Utah, *J. Atmos. Terr. Phys.*, *57*, 995–1008, 1995.

Fleming, E.L., S. Chandra, M.D. Burrage, W.R. Skinner, P.B. Hays, B.H. Solheim, and G.G. Shepherd, Climatological mean wind observations from the UARS high-resolution Doppler imager and wind imaging interferometer: Comparison with current reference models, *J. Geophys. Res.*, *101*, 10455–10473, 1996.

Franke, S.J., and D. Thorsen, Mean winds and tides in the upper middle atmosphere at Urbana (40°N, 88°W) during 1991-1992, *J. Geophys. Res.*, *98*, 18607–18615, 1993.

Fritts, D.C., and R.A. Vincent, Mesospheric momentum flux studies at Adelaide, Australia: Observations and a gravity wave-tidal interaction model, *J. Atmos. Sci.*, *44*, 605–619, 1987.

Fritts, D.C., and G.D. Nastrom, Sources of mesoscale variability of gravity waves. Part II: Frontal, convective, and jet stream excitation, *J. Atmos. Sci.*, *49*, 111–127, 1992.

Gao, X., J.W. Meriwether, V.B. Wickwar, and T.D. Wilkerson, Rayleigh lidar measurements of the temporal and vertical wavenumber spectra in the mesosphere height over the Rocky Mountain region, submitted, *J. Geophys. Res.*, 1997.

Garcia, R.R., and S. Solomon, The effect of breaking gravity waves on the dynamics and chemical composition of the mesosphere and lower thermosphere, *J. Geophys. Res.*, *90*, 3850–3868, 1985.

Geller, M.A., Dynamics of the middle atmosphere, *Space Sci. Rev.*, *34*, 359–375, 1983.

Hagan, M.E., J.M. Forbes, and F. Vial, On modeling migrating solar tides, *Geophys. Res. Lett.*, *22*, 893–896, 1995.

Hauchecorne, A., and M.-L. Chanin, A mid-latitude ground-based lidar study of stratospheric warmings and planetary wave propagation, *J. Atmos. Terr. Phys.*, *44*, 577–583, 1982.

Hauchecorne, A., and M.-L. Chanin, Mid-latitude lidar observations of planetary waves in the middle atmosphere during the winter of 1981–1982, *J. Geophys. Res.*, *88*, 3843–3849, 1983.

Hauchecorne, A., M.-L. Chanin, and R. Wilson, Mesospheric temperature inversion and gravity wave breaking, *Geophys. Res. Lett.*, *14*, 933–936, 1987.

Hauchecorne, A., M.-L. Chanin, and P. Keckhut, Climatology and trends of the middle atmospheric temperature (33–87 km) as seen by Rayleigh lidar over the south of France, *J. Geophys. Res.*, *96*, 15297–15309, 1991.

Hedin, A.E., E.L. Fleming, A.H. Manson, F.J. Schmidlin, S.K. Avery, R.R. Clark, S.J. Franke, G.J. Fraser, T. Tsuda, F. Vial, and R.A. Vincent, Empirical wind model for the upper, middle and lower atmosphere, *J. Atmos. Terr. Phys.*, *58*, 1421–1447, 1996.

Holton, J.R., The influence of gravity wave breaking on the general circulation of the middle atmosphere, *J. Atmos. Sci.*, *40*, 2497–2507, 1983.

Lindzen, R.S., Turbulences and stress owing to gravity wave and tidal breakdown, *J. Geophys. Res.*, *86*, 9707–9714, 1981.

Lowe, R.P., L.M. LeBlanc, and K.L. Gilbert, WINDII/UARS observation of twilight behaviour of the hydroxyl airglow, at mid-latitude equinox, *J. Atmos. Terr. Phys.*, *58*, 1863–1869, 1996.

Luo, Z., D.C. Fritts, R.W. Portmann, and G.E. Thomas, Dynamical and radiative forcing of the summer mesopause circulation and thermal structure, Part II: Seasonal variations, *J. Geophys. Res.*, *100*, 3129–3137, 1995.

Manson, A.H., C.E. Meek, H. Teitelbaum, F. Vial, R. Schminder, D. Kurschner, M.J. Smith, G.J. Fraser, and R.R. Clark, Climatologies of semi-diurnal and diurnal tides in the middle atmosphere (70–110 km) at middle latitudes (40-55), *J. Atmos. Terr. Phys.*, *51*, 579–593, 1989.

Marsh, A.K.P., N.J. Mitchell, and L. Thomas, Lidar studies of stratospheric gravity-wave spectra, *Planet. Space Sci.*, *39*, 1541–1548, 1991.

Mitchell, N.J., L. Thomas, and A.K.P. Marsh, Lidar observations of long-period gravity waves in the stratosphere, *Ann. Geophys.*, *9*, 588–596, 1991.

Miyahara, S., and J.M. Forbes, Theory and modeling tide/gravity-wave/mean-flow interactions in the mesosphere and lower thermosphere, *Adv. Space. Res.*, *12*, (10)7–(10)16, 1992.

Monson, I.K., The Fabry-Perot interferometer at Bear Lake Observatory—Improvements to the Data Reduction and Applications to OH and $O(^1D)$ Measurements, M.S. thesis, Utah State University, Logan, Utah, 1997.

Murayama, Y., T. Tsuda, and S. Fukao, Seasonal variation of gravity wave activity in the lower atmosphere observed with the MU radar, *J. Geophys. Res.*, *99*, 23057–23069, 1994a.

Murayama, Y., T. Tsuda, R. Wilson, H. Nakane, S.A. Hayashida, N. Sugimoto, I. Matsui, and Y. Sasano, Gravity wave activity in the upper atmosphere and lower mesosphere observed with the Rayleigh lidar at Tsukuba, Japan, *Geophys. Res. Lett.*, *21*, 1539–1542, 1994b.

Murgatoyd, R.J., Winds and temperatures between 20 km and 100 km—A review, *Quart. J. Roy. Meteor. Soc.*, *83*, 417–458, 1957.

Nastrom, G.D., and D.C. Fritts, Sources of mesoscale variability of gravity waves. Part I: Topographic excitation, *J. Atmos. Sci.*, *49*, 101–110, 1992.

Niciejewski, R.J., and T.L. Killeen, Nocturnal observations of the semidiurnal tide at a midlatitude site, *J. Geophys. Res.*, *100*, 25855–25866, 1995.

Rees, D., I. McWhirter, A. Aruliah, and S. Batten, Upper Atmospheric Wind and Temperature Measurements Using Imaging Fabry-Perot Interferometers, in *WITS Handbook,*, edited by C.H. Liu, pp. 188–223, Urbana, IL, 1989.

Rees, D., A. Aruliah, T.J. Fuller-Rowell, V.B. Wickwar, and R.J. Sica, Winds in the upper mesosphere at mid-latitude: First results using an imaging Fabry-Perot interferometer, *Geophys. Res. Lett.*, *17*, 1259–1262, 1990.

Reid, I.M., and R.A. Vincent, Measurements of the horizontal scales and phase velocities of short period mesosopheric gravity waves at Adelaide, Australia, *J. Atmos. Terr. Phys.*, *49*, 1033–1048, 1987.

Sears, R.D., T.D. Wilkerson, V.B. Wickwar, J.M. Maloney, and S.C. Collins, Multi-dimensional power spectral analysis of structure in the stratosphere and mesosphere observed by Rayleigh Scatter lidar, in *Advances in Atmospheric Remote Sensing with Lidar*, Ed. A. Ansmann, R. Neuber, P. Rairoux, and U. Wandinger, 561–564, Springer Verlag, Berlin, 1997.

Senft, D.C., G.C. Papen, C.S. Gardner, J.R. Yu, D.A. Krueger, and C.Y. She, Seasonal variations of the thermal structure of the mesopause region at Urbana, IL (40° N, 88° W) and Ft. Collins, CO (41° N, 105° W), *Geophys. Res. Lett.*, *21*, 821–824, 1994.

Smith, A.K., Longitudinal variations in mesospheric winds: Evidence for gravity wave filtering by planetary waves, *J. Atmos. Sci.*, *53*, 1156–1173, 1996.

Swenson, G.R., and S.B. Mende, OH emission and gravity waves (including a breaking wave) in all-sky imagery from Bear Lake, UT, *Geophys. Res. Lett.*, *21*, 2239–2242, 1994.

Thomas, L., and A.J. McDonald, The vertical propagation of gravity waves to lower mesospheric heights, in *Advances in Atmospheric Remote Sensing with Lidar*, Ed. by A. Ansmann, R. Neuber, P. Rairoux, and U. Wandinger, 565–568, Springer Verlag, Berlin, 1997.

Tsuda, T., Y. Murayama, M. Yamamoto, S. Kato, and S. Fukao, Seasonal variation of momentum flux in the mesosphere observed with the MU radar, *Geophys. Res. Lett.*, *17*, 725–728, 1990.

Tsuda, T., Y. Murayama, T. Nakamura, R.A. Vincent, A.H. Manson, C.E. Meek, and R.L. Wilson, Variations of the gravity wave characteristics with height, season and latitude revealed by comparative observations, *J. Atmos. Terr. Phys.*, *56*, 555–568, 1994.

Vadnais, C.M., Mesopause winds and OH intensities at mid-latitudes—Fabry-Perot Interferometer observations of the OH emission at 8430Å from Bear Lake Observatory, M.S. thesis, Utah State University, Logan, Utah, 1993.

Vial, F., Causes of Tidal Variability, in *Coupling Processes in the Lower and Middle Atmosphere*, edited by E.V. Thrane et al., pp. 137–151, Kluwer Academic Publishers, Netherlands, 1993.

Vincent, R.A., and D.C. Fritts, A climatology of gravity wave motions in the mesopause region at Adelaide, Australia, *J. Atmos. Sci.*, *44*, 748–760, 1987.

von Zahn, U., K.H. Fricke, R. Gerndt, and T. Blix, Mesospheric temperatures and the OH layer height as derived from ground-based lidar and OH* spectrometry, *J. Atmos. Terr. Phys.*, *49*, 863–869, 1987.

Wang, D.-Y., and D.C. Fritts, Evidence of gravity wave-tidal interaction observed near the summer mesopause at Poker Flat, Alaska, *J. Atmos. Sci.*, *48*, 572–583, 1991.

Westbrook, J.K., Extraplolation of Surface-Air Temperatures in Remote Areas Using Upper-Air Data, M.S. thesis, Utah State University, Logan, Utah, 1980.

Whiteway, J.A., and A.I. Carswell, Lidar observations of gravity wave activity in the upper stratosphere over Toronto, *J. Geophys. Res.*, *100*, 14113–14124, 1995.

Whiteway, J.A., A.I. Carswell, and W.E. Ward, Mesospheric temperature inversions with overlying nearly adiabatic lapse rate: an indication of a well-mixed turbulent layer, *Geophys. Res. Lett.*, *22*, 1201–1204, 1995.

Wickwar, V.B., T.D. Wilkerson, D. Rees, and S.C. Collins, Resonance lidar to study temperatures, winds, and metal densities in the upper mesosphere and lower thermosphere, *The Cedar Post*, October, (29), 29–30, 1996.

Wickwar, V.B., K.C. Beissner, S. Elkington, T.D. Wilkerson, S.C. Collins, T.D. Wilkerson, J.W. Meriwether, and X. Gao, Mesospheric temperature profiles determined from Rayleigh-scatter lidar observations above Logan, Utah, Submitted to *J. Geophys. Res.*, 1997a.

Wickwar, V.B., K.C. Beissner, T.D. Wilkerson, S.C. Collins, J.M. Maloney, J. W. Meriwether, and X. Gao, Climatology of mesospheric temperature profiles observed with the Consortium Rayleigh-scatter lidar at Logan, Utah, in *Advances in Atmospheric Remote Sensing with Lidar*, Ed. A. Ansmann, R. Neuber, P. Rairoux, and U. Wandinger, 557–560, Springer Verlag, Berlin, 1997b.

Wickwar, V.B., C.M. Vadnais, I.K. Monson, D. Rees, $O(^1D)$ intensities and winds at Bear Lake Observatory during periods of moderate magnetic activity, to be submitted to *J. Geophys. Res.*, 1997c.

Wiens, R.H., S.P. Zhang, R.N. Peterson, and G.G. Shepherd, Tides in emission rate and temperature from the O_2 nightglow over Bear Lake Observatory, *Geophys. Res. Lett.*, *22*, 2637–2640, 1995.

Wilson, R., M.L. Chanin, and A. Hauchecorne, Gravity waves in the middle atmosphere observed by Rayleigh lidar. 2. Climatology, *J. Geophys. Res.*, *96*, 5169–5183, 1991.

Wu, Q., and T.L. Killeen, Seasonal dependence of mesospheric gravity waves (<100 km) at Peach Mountain Observatory, Michigan, *Geophys. Res. Lett.*, *23*, 2211–2214, 1996.

Figure 1. The imaging Fabry-Perot interferometer at Bear Lake Observatory.

Figure 2. Example of FPI data for OH observations on 14 September 1993. The data extend from shortly after sunset to shortly before dawn. (See text for conversion from UT to LT and LST.) (a) OH intensities for eight azimuths and zenith. (b) Background intensities for the same eight azimuths and zenith. (c) LOS speeds when looking north (solid line) and south (dashed line). Positive speeds in m/s are for motion away from the FPI. The $\pm 1\sigma$ error bars are located at the center times of the four-minute integrations. (d) The same as (c) but for the east (solid)–west (dashed) pair of LOS speeds. (e) The northeast (solid)–southwest (dashed) pair of LOS speeds. (f) The northwest (solid)–southeast (dashed) pair of LOS speeds. (g) Hodogram presentation of the vector velocities going clockwise from the first data point in the fourth quadrant to the last data point in the first quadrant. (h) The resolved meridional (solid line, positive to the north) and zonal (dashed line, positive to the east) components of the vector wind, derived from the LOS speeds interpolated to 0, 15, 30, and 45 minutes after each hour.

Figure 3. Example of the evolution of OH wind vector maps for the night of 5 September 1994. The circle of 300-km diameter is the region viewed for an emission layer at 87 km and an elevation angle of 30°. The vector wind at each position is derived from the LOS speed in that direction and the two LOS speeds obtained at ±45° in azimuth. The velocity scale in m/s is given in the bottom-right corner.

Figure 4. The OH wind climatology for BLO. The average diurnal variations of the meridional (solid lines, positive to the north) and zonal (dashed lines, positive to the east) components are presented in m/s. Approximately four years of data, acquired between September 1989 and June 1995 are included in each monthly average. The division of the year into three seasons and two transition periods is discussed in the text.

Figure 5. Single-year OH wind climatologies for three Septembers, Junes, and Januarys. The average diurnal variations of the meridional (solid lines, positive to the north) and zonal (dashed lines, positive to the east) components are given in m/s.

Figure 6 . Examples of the variability of OH winds for six individual nights in *late summer*. The diurnal variation of the meridional (solid lines, positive to the north) and zonal (dashed lines, positive to the east) components are given in m/s.

Figure 7. Examples of the variability of OH winds for six individual nights in *summer*. The diurnal variation of the meridional (solid lines, positive to the north) and zonal (dashed lines, positive to the east) components are given in m/s. (As discussed in the text, the error bars shown for the June 1992 and July 1992 days are too big.)

Figure 8. Examples of the variability of OH winds for six individual nights in *winter*. The diurnal variation of the meridional (solid lines, positive to the north) and zonal (dashed lines, positive to the east) components are given in m/s. (As discussed in the text, the error bars shown for the January 1992 days are too big.)

Figure 9. Climatology of background wind and semidiurnal tide for FPI observations of OH at BLO. The top panel gives the background meridional wind (solid line, positive to the north) and the background zonal wind (dashed line, positive to the east) in m/s. The middle panel gives the amplitude of the meridional component of the semidiurnal tide (solid line, positive to the north) and the amplitude of the zonal component (dashed line, positive to the east) in m/s. Dotted lines are used for the months where data are unavailable. The bottom panel gives the UT of the minimum in the semidiurnal tide (the solid line, meridional component; dashed line, zonal component). The phase in LST is obtained by subtracting 1.4 hours. Dashed lines are used for the months where data are unavailable. Asterisks are used for additional data points in winter that have greater uncertainty.

Figure 10. Thirty-year average (1946–1975) of the prevailing wind speed just above the mountains (700 mbar) over BLO. (Adapted from *Westbrook*, 1980.)

Table 1. OH Wind Observations

Month	Years	Nights
January	4	37
February	4	31
March	4	30
April	4	24
May	4	30
June	4	28
July	3	24
August	3	32
September	4	30
October	3	26
November	4	24
December	4	42

Table 2. OH Climatological Seasons

Season	Months
Summer	May–July
Late Summer	August & September
Winter	November–February

Table 3. Deduced background winds and semidiurnal tides for 87 km at BLO

	Background Wind		Semidiurnal Tide			
Month	North	East	North		East	
	m/s	m/s	m/s	hrs	m/s	hrs
May	−11	8	15	4.9	12	7.3
June	−10	14	17	4.8	8	7.8
July	−10	14	20	4.5	13	8.2
Aug.	−6	15	26	3.6	23	6.5
Sept.	−2	4	28	3.6	25	5.9
Oct.	−7	1	14	1.6	9	5.1
Nov.	2	10	—	—	—	—
Dec.	8	5	5	6.6	8	10.6
Jan.	9	6	5	5.6	7	8.9
Feb.	9	4	—	—	—	—
Mar.	−2	−4	—	—	—	—
Apr.	−5	−6	12	4.8	12	6.4

Table 4. Day-to-day variability

Season	Variability[1]
Winter	Extremely Variable
Summer	Highly Variable
Late Summer	Very Similar

[1]Qualitative characterization. See, for instance, Figures 6–8.

Table 5. GSWM Tidal Climatologies for 42°N and 86 km[1]

	Semidiurnal Tide				Diurnal Tide			
Month	North		East		North		East	
	m/s	hrs	m/s	hrs	m/s	hrs	m/s	hrs
January	9.4	08.9	10.5	12.0	6.1	07.3	6.4	11.8
April	3.5	06.1	3.6	09.1	15.0	11.4	12.4	16.5
July	4.0	05.0	3.0	08.2	16.8	12.0	14.3	17.1
October	6.6	10.1	4.6	13.0	14.6	09.8	13.2	14.7

[1]Private Communication, M. Hagan, January 1997.

Table 6. Summary of the OH winds at BLO and middle atmosphere features that help to account for them*

Seasons	*Summer*	*Late Summer*	Transition	*Winter*	Transition
Mesosphere	Frequent GW images—eastward phase speed	Few GW images—eastward phase speed	No GW images	No GW images	Few GW images—eastward phase speed
	Strong eastward OH wind (12 m/s) **Strong southward OH wind (10 m/s)** **Strong SD tide (11/18 m/s)**	**Eastward OH wind (10 m/s)** **Southward OH wind (4 m/s)** **Very strong SD tide (24/27 m/s)**	**No zonal OH wind** **Southward OH wind (7 m/s)** **SD tide (9/14 m/s)**	**Weak eastward OH wind (6 m/s)** **Northward OH wind (7 m/s)** **Weak SD tide (8/5 m/s)**	**Weak westward OH wind (5 m/s)** **Weak southward OH wind (4 m/s)** **SD tide (12/12 m/s in April)**
	Maximum in GW activity			Smaller max. in GW activity	
	Strong westward jet	West-to-east jet reversal	Eastward jet	Strong eastward jet	East-to-west jet reversal
	Decelerate westward flow and accelerate to the east			Decelerate eastward flow	
	Breaking GWs with eastward phase speeds in meso. & lower thermo.			Possible strong PW influence	
Stratosphere	Filter GWs with westward phase speed, if they exist	Filter GWs with eastward phase speed when mesospheric jet is eastward	Filter GWs with eastward phase speed	Filter GWs with eastward phase speed	Filter GWs with eastward phase speed when mesospheric jet is eastward
	Minimum in GW activity	Minimum in GW activity		Maximum in GW activity	
	SD O_3 tidal source	SD O_3 tidal source	SD O_3 tidal source	SD O_3 tidal source	SD O_3 tidal source
	Filter GWs with zero phase speed	Filter GWs with zero phase speed when mesospheric jet is westward		Breaking GWs with zero phase speed in stratosphere & mesosphere	Filter GWs with zero phase speed when mesospheric jet is westward
Troposphere	Eastward jet & GW source	Weak eastward jet & weak GW source	Eastward jet & GW source	Strong eastward jet & strong GW source	Eastward jet & GW source
	SD H_2O tidal source	SD H_2O tidal source	SD H_2O tidal source	SD H_2O tidal source	SD H_2O tidal source
	Very weak topographic GW source (3.9 m/s)	Weak topographic GW source (5.8 m/s)	Topographic GW source (7.4 m/s)	Strong topographic GW source (14.4 m/s)	Topographic GW source (7.3 m/s)

* SD = semidiurnal GW = gravity wave PW = planetary wave. Items in bold refer to the BLO observations. "x/y m/s" refers to a zonal amplitude of x and a meridional amplitude of y.

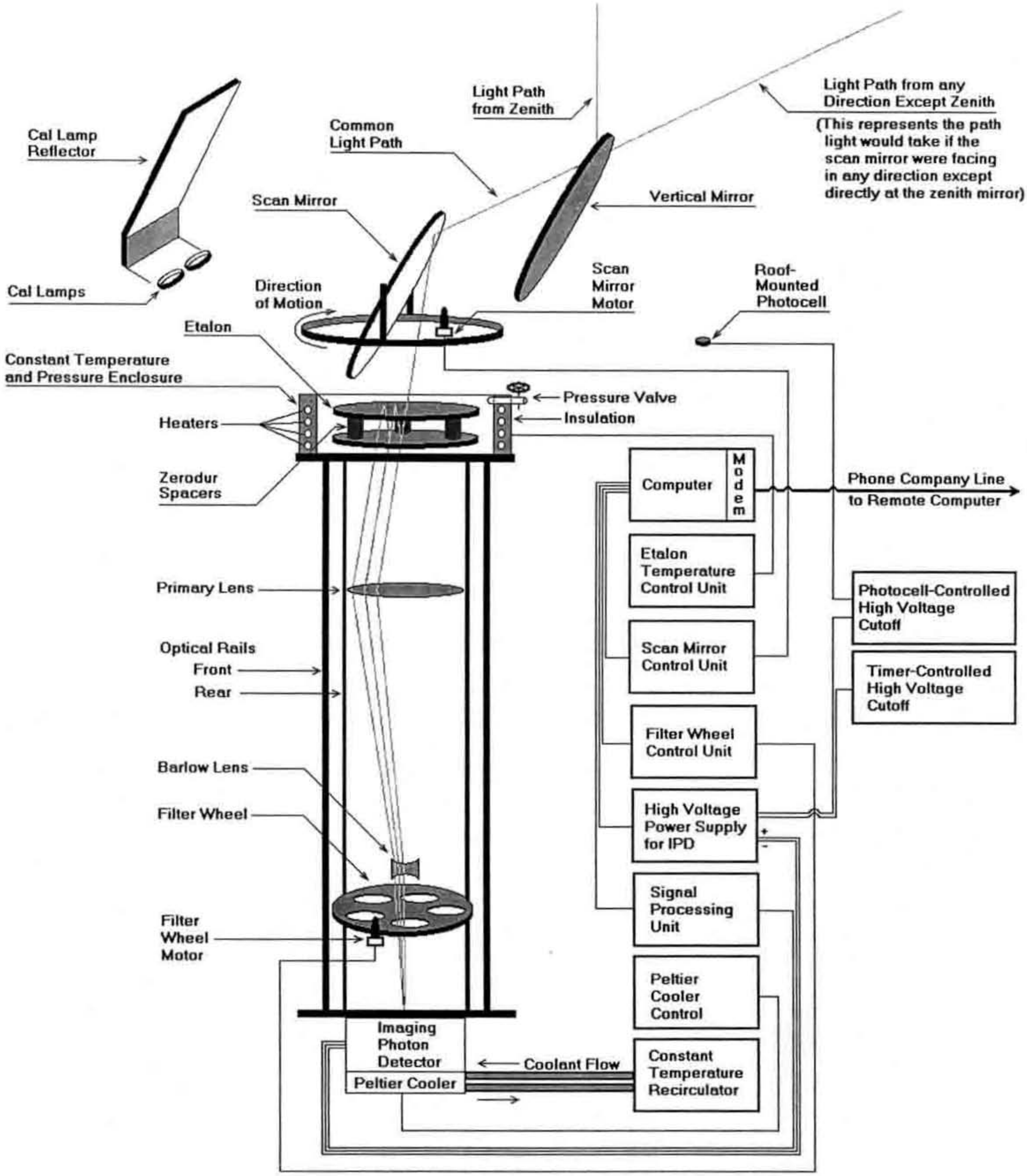

Light Path from Zenith
Light Path from any Direction Except Zenith
(This represents the path light would take if the scan mirror were facing in any direction except directly at the zenith mirror)
Cal Lamp Reflector
Common Light Path
Vertical Mirror
Scan Mirror
Cal Lamps
Direction of Motion
Scan Mirror Motor
Roof-Mounted Photocell
Etalon
Constant Temperature and Pressure Enclosure
Pressure Valve
Insulation
Heaters
Zerodur Spacers
Computer
Modem
Phone Company Line to Remote Computer
Etalon Temperature Control Unit
Primary Lens
Photocell-Controlled High Voltage Cutoff
Optical Rails
Front
Rear
Scan Mirror Control Unit
Timer-Controlled High Voltage Cutoff
Filter Wheel Control Unit
Barlow Lens
Filter Wheel
High Voltage Power Supply for IPD
+
-
Signal Processing Unit
Filter Wheel Motor
Peltier Cooler Control
Imaging Photon Detector
Peltier Cooler
Coolant Flow
Constant Temperature Recirculator

Figure 1

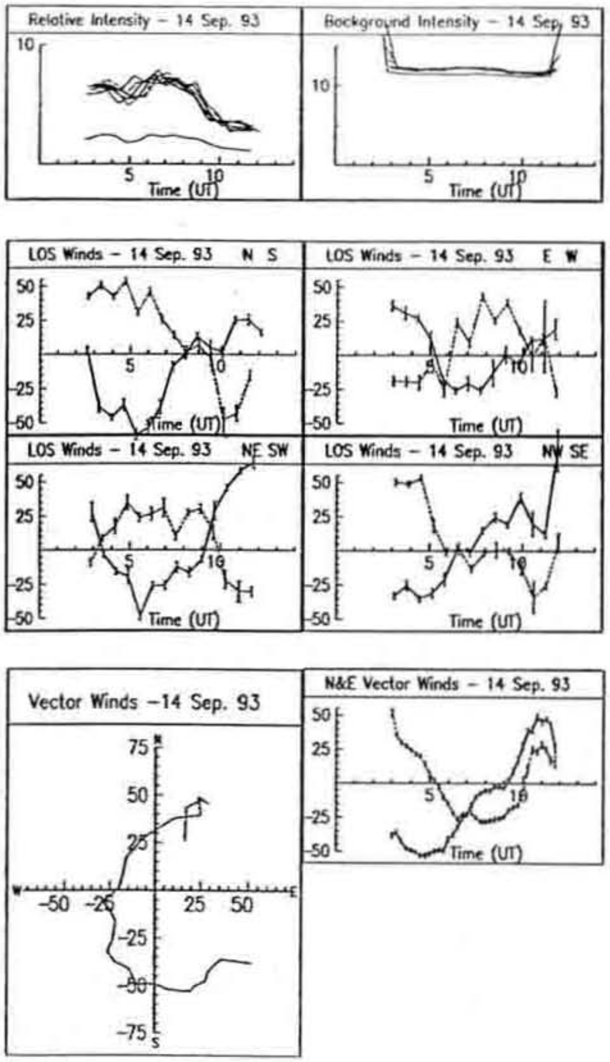
Relative Intensity - 14 Sep. 93
Background Intensity - 14 Sep. 93
LOS Winds - 14 Sep. 93 N S
LOS Winds - 14 Sep. 93 E W
LOS Winds - 14 Sep. 93 NE SW
LOS Winds - 14 Sep. 93 NW SE
Vector Winds -14 Sep. 93
N&E Vector Winds - 14 Sep. 93
Time (UT)

Figure 2

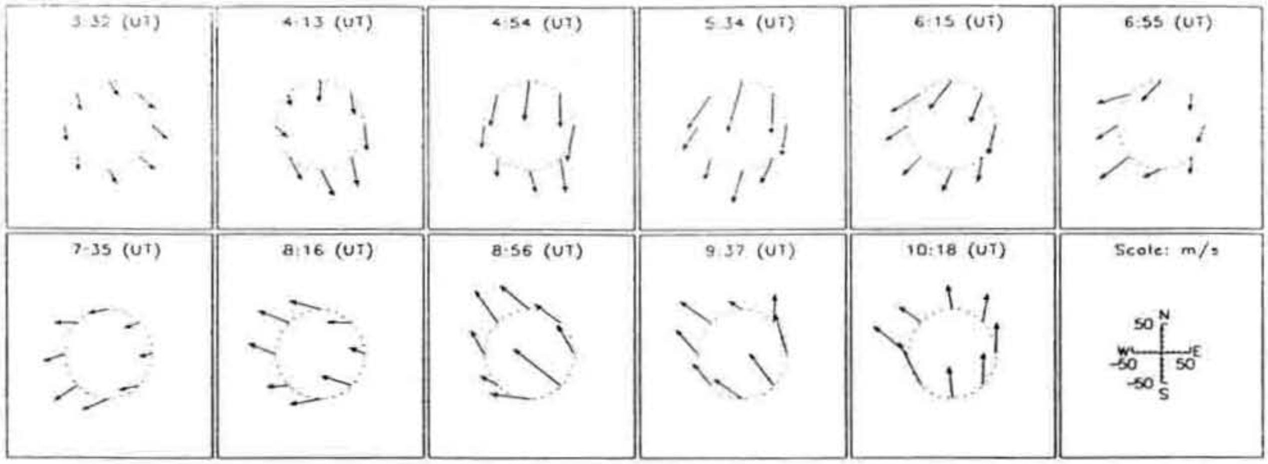
3:32 (UT)
4:13 (UT)
4:54 (UT)
5:34 (UT)
6:15 (UT)
6:55 (UT)
7:35 (UT)
8:16 (UT)
8:56 (UT)
9:37 (UT)
10:18 (UT)
Scale: m/s
50
N
W
-50
E
50
-50
S

Figure 3

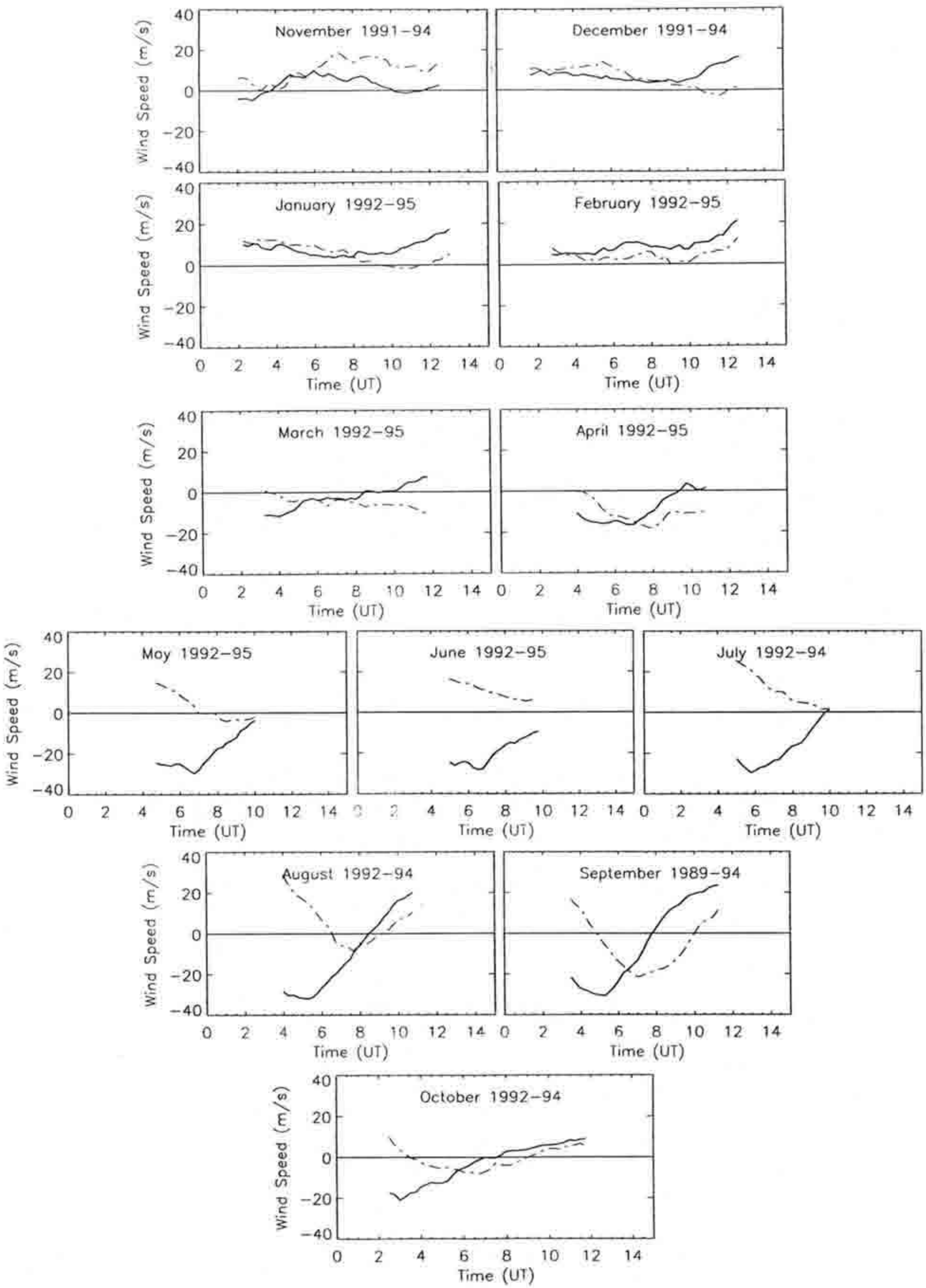

November 1991-94
December 1991-94
January 1992-95
February 1992-95
March 1992-95
April 1992-95
May 1992-95
June 1992-95
July 1992-94
August 1992-94
September 1989-94
October 1992-94
Wind Speed (m/s)
Time (UT)

Figure 4

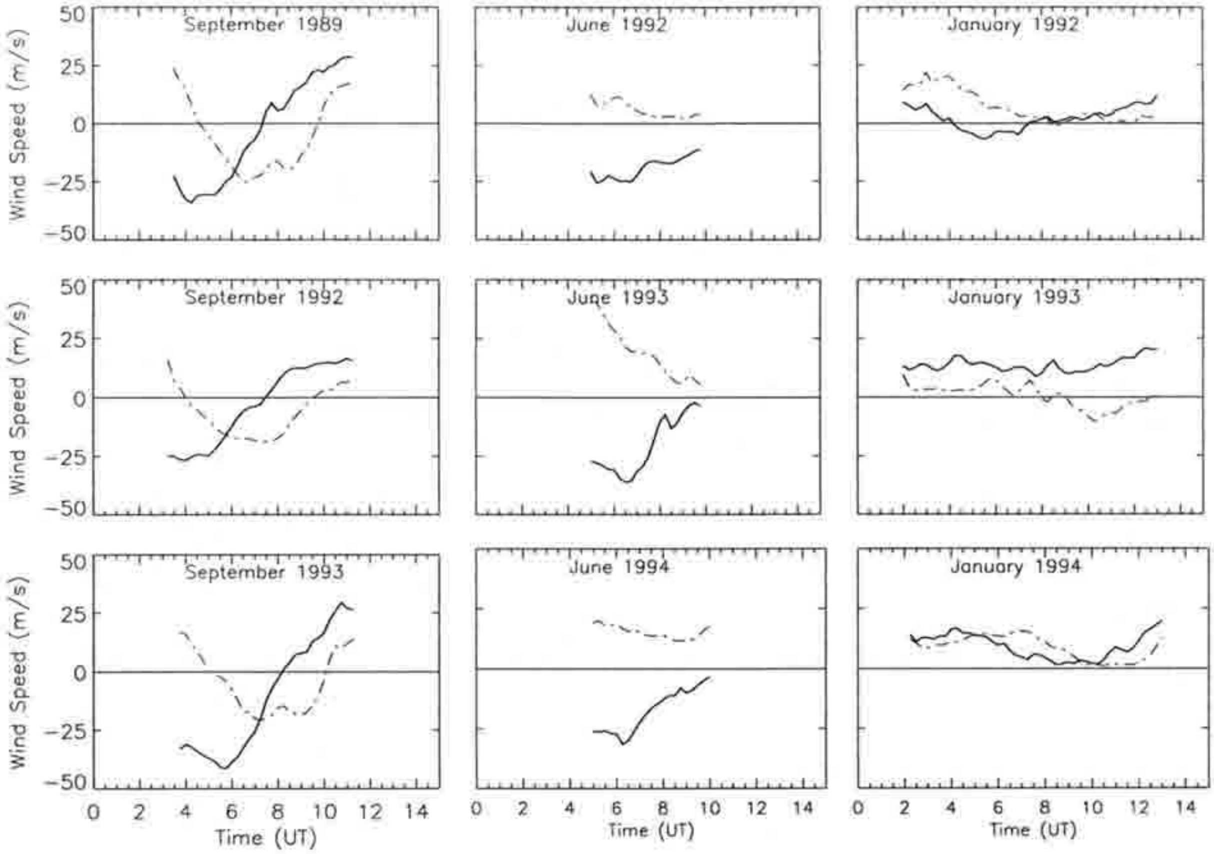
September 1989
June 1992
January 1992
September 1992
June 1993
January 1993
September 1993
June 1994
January 1994
Wind Speed (m/s)
Time (UT)
50
25
0
-25
-50
0
2
4
6
8
10
12
14

Figure 5

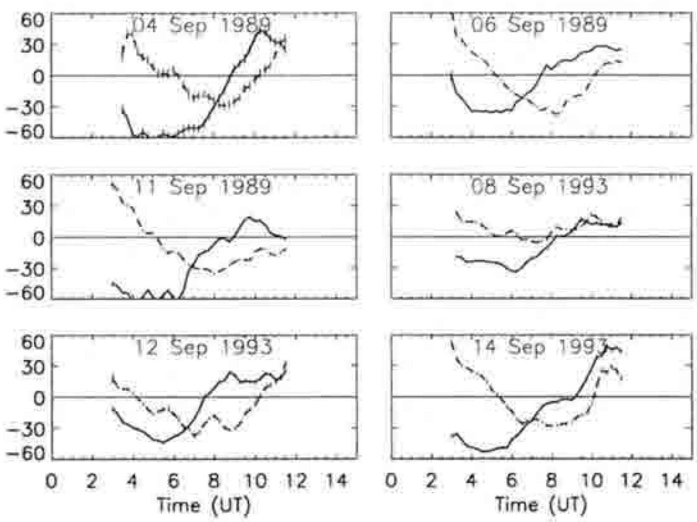
04 Sep 1989
06 Sep 1989
11 Sep 1989
08 Sep 1993
12 Sep 1993
14 Sep 1993
Time (UT)
Time (UT)

Figure 6

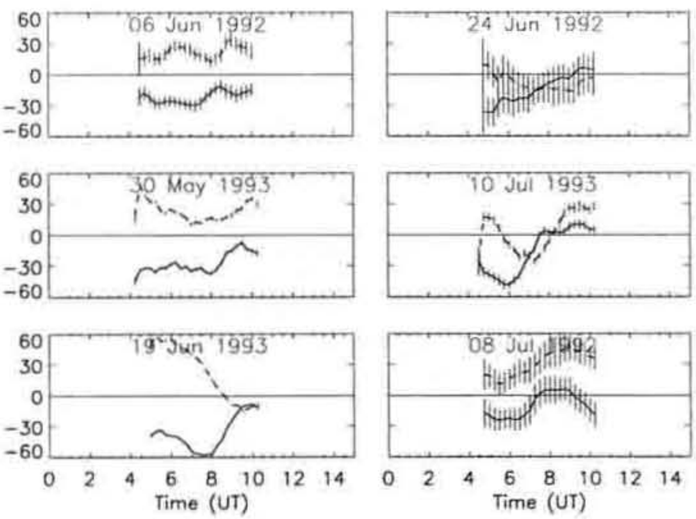

06 Jun 1992
24 Jun 1992
30 May 1993
10 Jul 1993
19 Jun 1993
08 Jul 1992
60
30
0
−30
−60
0 2 4 6 8 10 12 14
Time (UT)

Figure 7

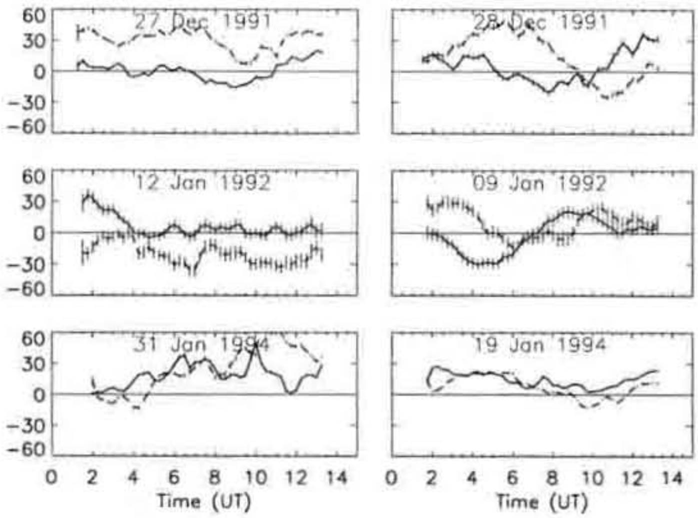
27 Dec 1991
28 Dec 1991
12 Jan 1992
09 Jan 1992
31 Jan 1994
19 Jan 1994
60
30
0
−30
−60
0 2 4 6 8 10 12 14
Time (UT)

Figure 8

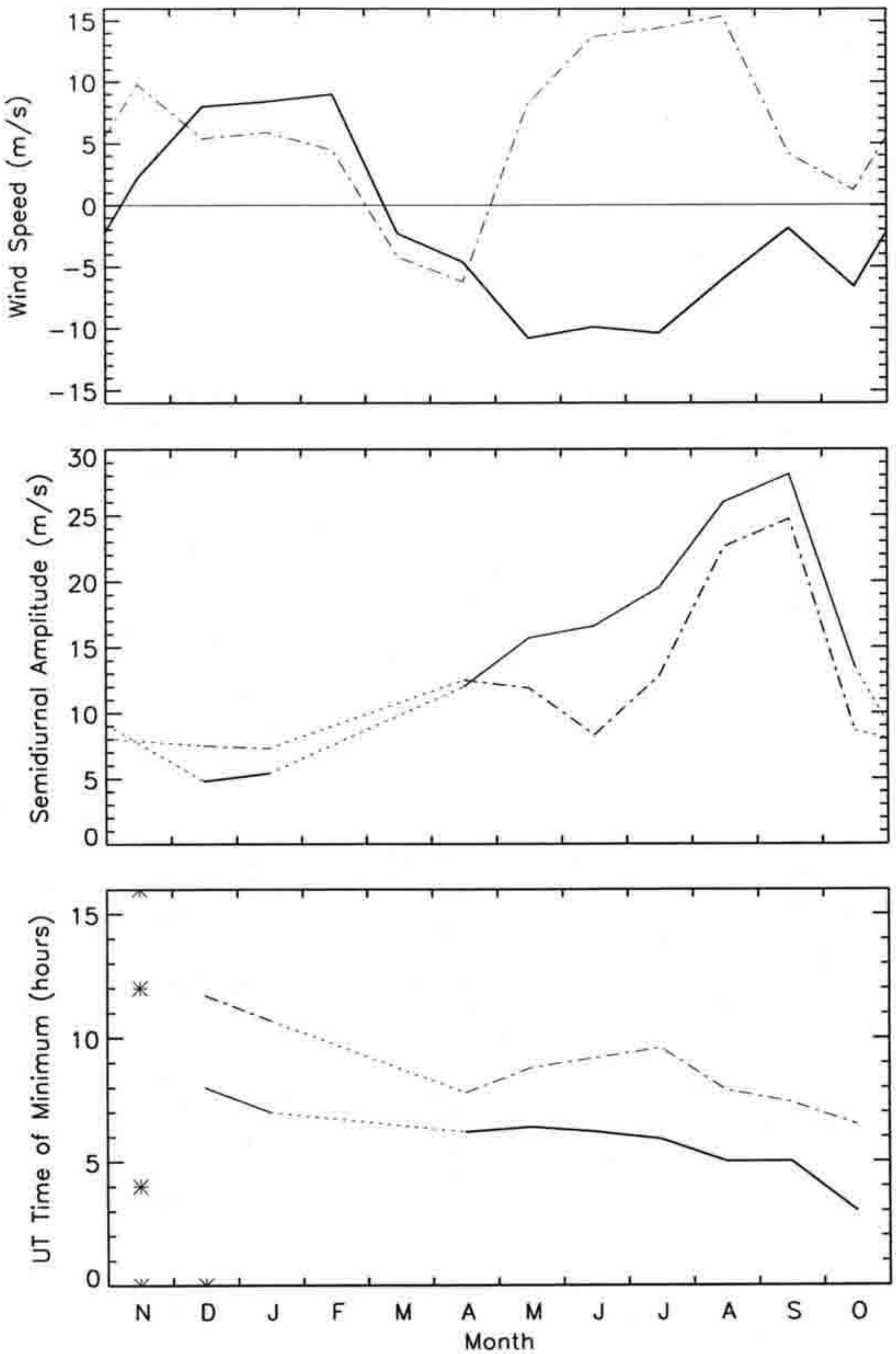
Wind Speed (m/s)
15
10
5
0
−5
−10
−15
Semidiurnal Amplitude (m/s)
30
25
20
15
10
5
0
UT Time of Minimum (hours)
15
10
5
0
N
D
J
F
M
A
M
J
J
A
S
O
Month

Figure 9

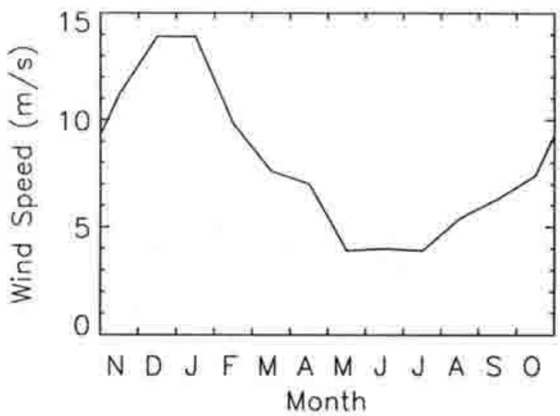

Figure 10